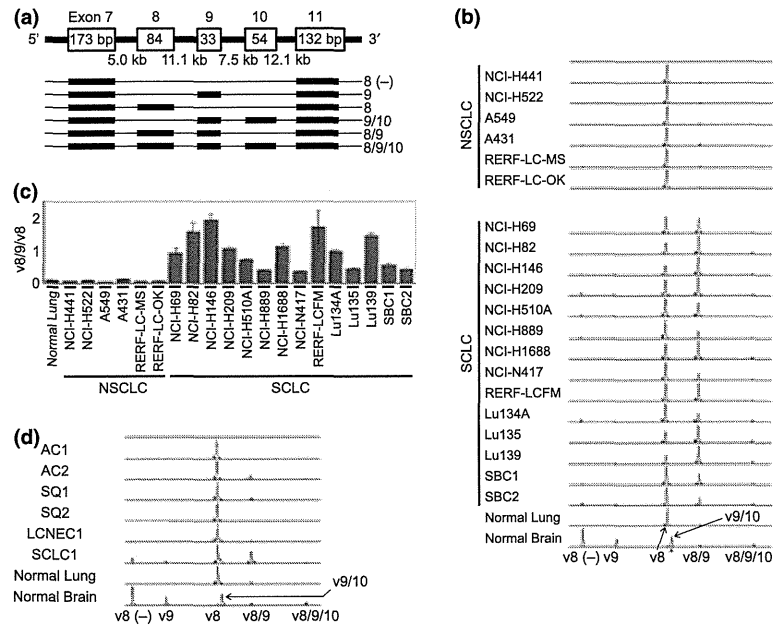

Fig. 2. Splicing variants of CADM1 mRNA. (a) Schematic representation of six splicing variants of CADM1. Boxes indicate exons with their nucleotide length, while bars indicate introns with their length (not in scale). (b) Splicing variants of CADM1 in small cell lung cancer (SCLC) and non-SCLC (NSCLC) cells and human lung and brain by RT-PCR analysis followed by PAGE with 6 M urea. Note that peaks within the same specimens are quantitative, but the peaks between the specimens are not. (c) Ratio of variant 8/9 to variant 8 of CADM1 mRNA in samples shown in (b). Columns represent the mean ± SD (bars). The data were obtained from three independent experiments. (d) Splicing variants in primary lung cancers by RT-PCR analysis. AD, SQ and LCNEC indicate adenocarcinoma, squamous cell carcinoma and large cell neuroendocrine carcinoma, respectively.

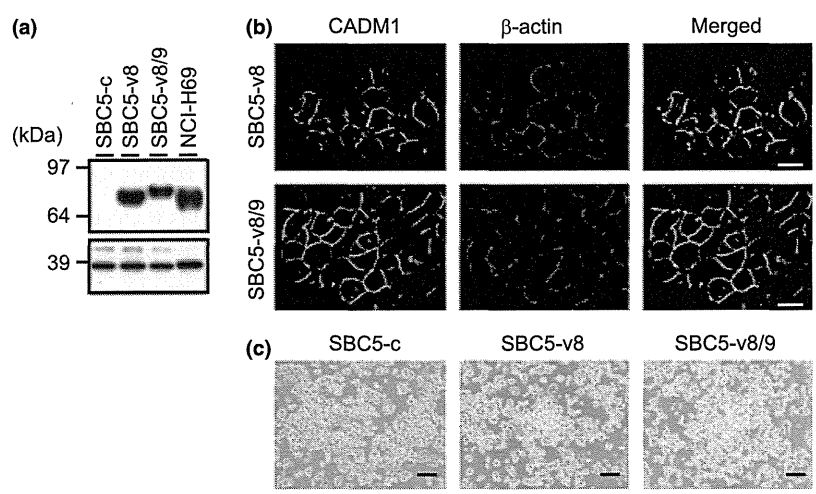

Fig. 3. Cell aggregation activity of CADM1 in small cell lung cancer (SCLC) cells. (a) Exogenous expression of variant 8 and variant 8/9 of CADM1 (upper) and GAPDH (lower) in SCLC cells, SBC5, detected by western blotting. (b) Expression of variant 8 and variant 8/9 of CADM1 protein in cell to cell attachment sites in SBC5 cells. CADM1 (green) and beta-actin (red) were detected as described in the Materials and Methods, and merged images of the left and middle panels are shown on the right. Bar represents 20 μm. (c) Morphology of SBC5-c (left), SBC5-v8 (middle) and SBC5-v8/9 (right) cells under phase-contrast microscopy. Bar indicates 100 μm.

suggest that CADM1 might play a role in the formation of large 3-D spheroids of SCLC cells *in vitro*.

Discussion

The present study demonstrates that CADM1 could provide a promising target for both the diagnosis and treatment of SCLC because CADM1 is a membrane protein. For possible diagnosis, splicing variant 8/9 of CADM1 could be a promising marker of SCLC. As shown in Fig. 1, the CADM1 protein is expressed in 11 of 16 (69%) SCLC cells and 10 of 35 (29%) primary SCLC tumors. Furthermore, we found that all SCLC cells expressed a unique variant 8/9 of CADM1 in addition to a variant 8, commonly expressed in the epithelia. Considering its specific expression in SCLC and testis, variant 8/9 would be a very promising candidate as a diagnostic marker of

doi: 10.1111/j.1349-7006.2012.02277.x

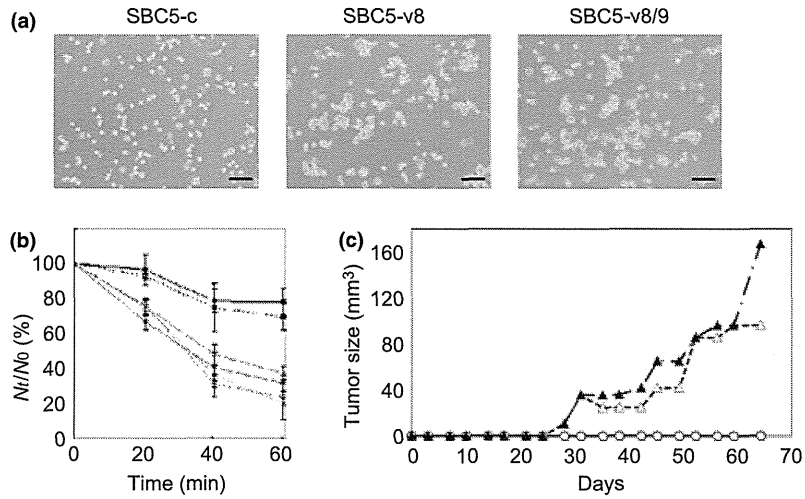

Fig. 4. Enhanced aggregation and tumorigenicity of SBC5 cells by CADM1. (a) Morphology of SBC5-c (left), SBC5-v8 (middle) and SBC5-v8/9 cells (right) in Ca^{2+}-free and Mg^{2+}-free HBSS. Bar represents 100 μm. (b) Ca^{2+}-independent and Mg^{2+}-independent aggregation activity of CADM1 in small cell lung cancer (SCLC). SBC5-v8 (blue circles), SBC5-v8/9 (red triangles) and SBC5-c (black squares) were treated with trypsine/EDTA and rotated in HBSS containing Ca^{2+} and Mg^{2+} (dotted lines) or Ca^{2+}-free and Mg^{2+}-free HBSS (solid lines). The average ratio (N_t/N_0) in triplicate experiments was indicated. (c) Subcutaneous tumor formation in Balb/c nu/nu mice. 1×10^6 of SBC5-v8 (dotted line with open triangles), SBC5-v8/9 (dashed line with closed triangles) and SBC5-c (black line with open circles) cells were injected, and the average volume of tumors was determined at the indicated times after injection.

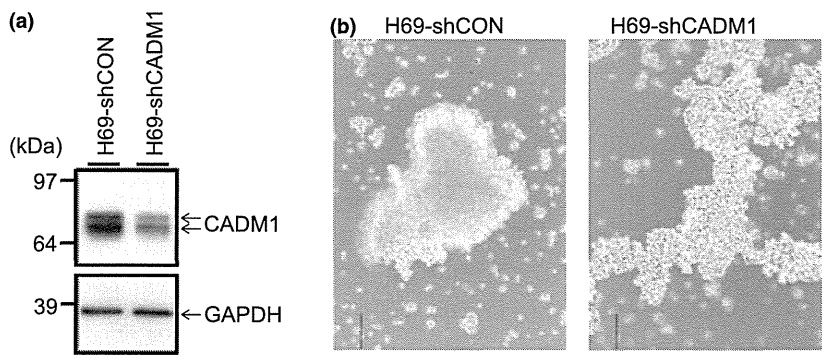

Fig. 5. Abrogation of spheroid formation of NCI-H69 cells by shRNA of CADM1. (a) Western blotting of CADM1 in NCI-H69 cells transfected with shRNA against CADM1 (H69-shCADM1) and control shRNA (H69-shCON). (b) Representative pictures of H69-shCADM1 and H69-shCON cells in culture media.

SCLC. It is noteworthy, however, that a very small peak corresponding to variant 8/9 was also detected in mouse brain, esophagus, jejunum and kidney. A small peak might be derived from a small population of SCLC-precursor cells of neuroendocrine origin. Alternatively, variant 8/9 might be expressed as a minor isoform of CADM1 in cells from these tissues. In this study, we identified six splicing variants of CADM1, including two novel variants, variant 9 and variant 8/9/10. Variant 9 is expressed in the testis, colon and brain, whereas variant 8/9/10 is expressed as a small peak in the brain (Fig. S1). These variable fragments are located just outside the cell membrane of the CADM1 protein, connecting the domain of three immunoglobulin loops to the transmembrane domain as a possible hinge. It is noteworthy that cancer-specific splicing variants of CD44 also differ in the fragments just outside the cell membrane.[31] Exons 8, 9 and 10 of CADM1 contain 28, 11 and 18 amino acids, respectively, where exons 8 and 9 contain threonine-rich repeats that could be modified by O-glycosylation. The numbers of possible O-glycosylation sites in the fragments corresponding to exons 8, 9 and 10 are 16, 2 and 0, respectively.[29,30] Therefore, variants 8 and 8/9 contain 16 and 18 possible O-glycosylation sites, respectively, whereas variant 8(−), expressed in the brain, does not contain possible O-glycosylation sites. Therefore, variant 8(−) and variant 8 or 8/9 proteins would show a marked difference in a higher structure, whereas the difference between variants 8 and 8/9 might be less remarkable. CADM1 in SCLC is also highly glycosylated through N-glycosylation, as shown in Fig. 1c. However, the degree of glycosylation does not correlate with their malignant features in at least 4 SCLC cells examined. Thus, the pathological significance of N-glycosylation and O-glycosylation of CADM1 in SCLC remains unclear. These variants are also intriguing as a serum marker because the CADM1 protein shows possible shedding by several proteases, including ADAM10 and γ-secretase.[32] However, we were unable to investigate the pathological significance of CADM1 expression in primary SCLC because the paraffin sections of primary SCLC that we examined were provided commercially without detailed clinicopathological information.

This study also provides a possible therapeutic target of SCLC. Of 14 SCLC cell lines expressing CADM1, 11 showed spheroid growth *in vitro*. By contrast, CADM1 is not detected in 2 SCLC cells showing attached growth, strongly suggesting that CADM1 overexpression could promote anchorage-independent cell growth, one of the indicators of the malignant phenotype of cancer cells. CADM1, therefore, appears to act as an oncoprotein in SCLC, as it does in ATL, rather than a tumor suppressor. This hypothesis was supported by the following three findings in the present study: (i) CADM1 expression in SCLC cells correlated well with spheroid formation *in vitro*; (ii) introduction of CADM1 into SCLC cells enhanced aggregation *in vitro* and tumor formation in nude mice; (iii) suppression of CADM1 expression by shRNA reduced a population of spheroid growth *in vitro*. Spheroid growth of SCLC shown in this study is abrogated by serum depletion, indicating that this is not a feature of currently recognized cancer stem cells. However, the enhancement of cell aggregation *in vitro* and tumorigenicity *in vivo* by CADM1 indicate that CADM1 promotes the malignant features of SCLC, in contrast to NSCLC. The distinct roles of CADM1 in oncogenesis in SCLC and NSCLC would be due to the different downstream cascade in these two subtypes of lung cancer. One of the candidate downstream targets in SCLC is Tiam1, as observed in ATL,[26] although preliminary results show that Tiam1 protein is detected in both NCI-H69 cells expressing CADM1 with anchorage-independent proliferation and SBC5 cells lacking CADM1 with anchorage-dependent proliferation. Phosphoinositide 3-kinase (PI3K) is another possible downstream molecule. A previous study demonstrates that PI3K is constitutively active in SCLC and could mediate anchorage-independent proliferation of SCLC cells.[33] Furthermore, a subset of SCLC showed oncogenic mutation of the *PIK3CA* gene,[34] although possible crosstalk of CADM1 and PI3K is not yet demonstrated. Additional studies are required to obtain a better picture of the CADM1 cascades in SCLC. It is also noteworthy that instead of spheroids, sheet-like aggregation was predominantly observed in NCI-H69 when CADM1 expression was reduced. This sheet-like aggregation was further broken to generate tiny particles or single cells when treated with EDTA (data not shown). These findings suggest that CADM1 might play a role in 3-D spheroid aggregation, whereas 2-D sheet-like aggregation is mainly caused by Ca^{2+}-dependent cell–cell adhesion activities, including those by cadherins. In summary, we demonstrate that variant 8/9 of CADM1 is specifically expressed in SCLC and might promote spheroid-like cell growth and tumorigenicity, providing a possible molecular target for the diagnosis and treatment of SCLC.

Acknowledgments

This work was supported in part by a Grant-in-Aid for Young Scientists (B) (20790276, 22700914 for MI and 21790309 for MSY) and a Grant-in-Aid for Scientific Research (B) [22300336 for YM] from the Ministry of Education, Culture, Sports, Science, and Technology of Japan; a Grant-in-Aid for the Third-Term Comprehensive Control Research for Cancer from the Ministry of Health, Labor, and Welfare of Japan; and a Grant from the Program for the Promotion of Fundamental Studies in Health Sciences from the National Institute of Biomedical Innovation (ID05-10 for YM).

Disclosure Statement

The authors have no conflict of interest.

References

1 Komaki R. Combined treatment for limited small cell lung cancer. *Semin Oncol* 2003; **30**: 56–70.
2 Fried P, Wolf K. Tumour-cell invasion and migration: diversity and escape mechanisms. *Nat Rev Cancer* 2003; **3**: 362–72.
3 D'Angelo SP, Pietanza MC. The molecular pathogenesis of small cell lung cancer. *Cancer Biol Ther* 2010; **10**: 1–10.
4 Yokota J, Kohno T. Molecular footprints of human lung cancer progression. *Cancer Sci* 2004; **95**: 197–204.
5 Kohno T, Sakiyama T, Kunitoh H *et al.* Association of polymorphisms in the MTH1 gene with small cell lung carcinoma risk. *Carcinogenesis* 2006; **27**: 2448–54.
6 Kuramochi M, Fukuhara H, Nobukuni T *et al. TSLC1* is a tumor suppressor gene in human non-small cell lung cancer. *Nat Genet* 2001; **27**: 427–30.
7 Murakami Y. Functional cloning of a tumor suppressor gene, *TSLC1*, in human non-small cell lung cancer. *Oncogene* 2002; **21**: 6936–48.
8 Masuda M, Yageta M, Fukuhara H *et al.* The tumor suppressor protein-TSLC1 is involved in cell-cell adhesion. *J Biol Chem* 2002; **277**: 31014–9.
9 Kikuchi S, Yamada D, Fukami T *et al.* Hypermethylation of the TSLC1/IGSF4 promoter is associated with tobacco smoking and a poor prognosis in primary non-small cell lung cancer. *Cancer* 2006; **106**: 1751–8.
10 Fukuhara H, Kuramochi M, Fukami T *et al.* Promoter methylation of the*TSLC1* and tumor suppression by its gene product in human prostate cancer. *Jpn J Cancer Res* 2002; **93**: 605–9.
11 Allinen M, Peri L, Kujala S *et al.* Analysis of 11q21–24 loss of heterozygosity candidate target genes in breast cancer: indications of TSLC1 promoter hypermethylation. *Genes Chromosom Cancer* 2002; **34**: 384–9.
12 Jansen M, Fukushima N, Rosty C *et al.* Aberrant methylation of the 5′ CpG island of TSLC1 is common in pancreatic ductal adenocarcinoma and is first manifest in high-grade PanINs. *Cancer Biol Ther* 2002; **1**: 293–6.
13 Honda T, Tamura G, Waki T *et al.* Hypermethylation of the *TSLC1* gene promoter in primary gastric cancers and gastric cancer cell lines. *Jpn J Cancer Res* 2002; **93**: 857–60.
14 Ito T, Shimada Y, Hashimoto Y *et al.* Involvement of TSLC1 in progression of esophageal squamous cell carcinoma. *Cancer Res* 2003; **63**: 6320–6.
15 Lung H-L, Cheng Y, Kumaran MK *et al.* Fine mapping of 11q22–23tumor suppressive region and involvement of *TSLC1* in nasopharyngeal carcinoma. *Int J Cancer* 2004; **112**: 628–35.
16 Steenbergen RD, Kramer D, Braakhuis BJ *et al.* TSLC1 gene silencing in cervical cancer cell lines and cervical neoplasia. *J Natl Cancer Inst* 2004; **96**: 294–305.
17 Yageta M, Kuramochi M, Masuda M *et al.* Direct association of TSLC1and DAL-1, two distinct tumor suppressor proteins in lung cancer. *Cancer Res* 2002; **62**: 5129–33.
18 Fukuhara H, Masuda M, Yageta M *et al.* Association of a lung tumor suppressor TSLC1 with MPP3, a human homologue of drosophila tumor suppressor Dlg. *Oncogene* 2003; **22**: 6160–5.
19 Shingai T, Ikeda W, Kakunaga S *et al.* Implications of nectin-likemolecule-2/IGSF4/RA175/SgIGSF/TSLC1/SynCAM1 in cell–cell adhesion and transmembrane protein localization in epithelial cells. *J Biol Chem* 2003; **278**: 35421–7.
20 Sakurai-Yageta M, Masuda M, Tsuboi Y, Ito A, Murakami Y. Tumor suppressor CADM1 is involved in epithelial cell structure. *Biochem Biophys Res Commun* 2009; **390**: 977–82.
21 Gutmann DH, Donahoe J, Perry A *et al.* Loss of DAL-1, a protein 4.1-related tumor suppressor, is an important early event in the pathogenesis of meningiomas. *Hum Mol Genet* 2000; **9**: 1495–500.
22 Kikuchi S, Yamada D, Fukami T *et al.* Promoter methylation of the *DAL-1/4.1B* predicts poor prognosis in non-small cell lung cancer. *Clin Cancer Res* 2005; **11**: 2954–61.
23 Yamada D, Kikuchi S, Williams YN *et al.* Promoter hypermethylation of the potential tumor suppressor *DAL-1/4.1B* gene in renal clear cell carcinoma. *Int J Cancer* 2006; **118**: 916–23.
24 Sasaki H, Nishikata I, Shiraga T *et al.* Overexpression of a cell adhesion molecule, TSLC1, as a possible molecular marker for acute type of adult T-cell leukemia. *Blood* 2005; **105**: 1204–13.
25 Dewan MZ, Takamatsu N, Hidaka T *et al.* Critical role for TSLC1 expression in the growth and organ infiltration of adult T-cell leukemia cells in vitro. *J Virol* 2008; **82**: 11958–63.
26 Masuda M, Maruyama T, Ohta T *et al.* CADM1 interacts with Tiam1 and promotes invasive phenotype of human T-cell leukemia virus type I (HTLV-I) transformed cells and adult T-cell leukemia (ATL) cells. *J Biol Chem* 2010; **285**: 15511–22.

doi: 10.1111/j.1349-7006.2012.02277.x

27 Yamada D, Yoshida M, Williams YN *et al.* Disruption of spermatogenic cell adhesion and male infertility in mice lacking TSLC1/IGSF4, an immunoglobulin superfamily cell adhesion molecule. *Mol Cell Biol* 2006; **26**: 3610–24.
28 Takahashi Y, Iwai M, Kawai T *et al.* Aberrant expression of tumor suppressors, CADM1 and 4.1B, in invasive lesions of primary breast cancer. *Breast Cancer* 2011; doi: 10.1007/s12282-011-0272-7 [Epub ahead of print].
29 Murakami Y. Involvement of a cell adhesion molecule, TSLC1/IGSF4, in human oncogenesis. *Cancer Sci* 2005; **96**: 543–52.
30 Biederer T. Bioinformatic characterization of the SynCAM family of immunoglobulin-like domain-containing adhesion molecules. *Genomics* 2006; **87**: 139–50.
31 Nagano O, Saya H. Mechanism and biological significance of CD44 cleavage. *Cancer Sci* 2004; **95**: 930–5.
32 Nagara Y, Hagiyama M, Hatano N *et al.* Tumor suppressor cell adhesion molecule 1 (CADM1) is cleaved by a disintegrin and metalloprotease 10 (ADAM10) and subsequently cleaved by gamma-secretase complex. *Biochem Biophys Res Commun* 2012; **17**: 462–7.
33 Moore SM, Rintoul RC, Walker TR *et al.* The presence of a constitutively active phosphoinositide 3-kinase in small cell lung cancer cells mediates anchorage-independent proliferation via a protein kinase B and p70s6k-dependent pathway. *Cancer Res* 1998; **58**: 5239–47.
34 Shibata T, Kokubu A, Tsuta K, Hirohashi S. Oncogenic mutation of PIK3CA in small cell lung carcinoma: a potential therapeutic target pathway for chemotherapy-resistant lung cancer. *Cancer Lett* 2009; **283**: 203–11.

Supporting Information

Additional Supporting Information may be found in the online version of this article:

Fig. S1. RT-PCR analysis of CADM1 expression in small cell lung cancer (SCLC) and non-SCLC (NSCLC).

Fig. S2. Immunohistochemical analysis of CADM1 protein in primary small cell lung cancer.

Fig. S3. Splicing variants of CADM1 in various mouse tissues detected by RT-PCR followed by SDS-PAGE analysis.

Table S1. Cell lines examined.

Table S2. Numbers of cell subpopulations showing spheroids, sheet-like cell aggregates and small aggregates in H69-shCON and H69-shCADM1 cells.

Please note: Wiley-Blackwell are not responsible for the content or functionality of any supporting materials supplied by the authors. Any queries (other than missing material) should be directed to the corresponding author for the article.

Published OnlineFirst December 21, 2011; DOI:10.1158/1078-0432.CCR-11-1946

Human Cancer Biology

Clinical Cancer Research

Upregulation of Notch2 and Six1 Is Associated with Progression of Early-Stage Lung Adenocarcinoma and a More Aggressive Phenotype at Advanced Stages

Takahiro Mimae[1,2], Morihito Okada[1], Man Hagiyama[2,3], Yoshihiro Miyata[1], Yasuhiro Tsutani[1], Takao Inoue[3], Yoshinori Murakami[2], and Akihiko Ito[3]

Abstract

Purpose: Lung adenocarcinoma often manifests as tumors with mainly lepidic growth. The size of invasive foci determines a diagnosis of *in situ*, minimally invasive adenocarcinoma, or invasive types and suggests that some adenocarcinomas undergo malignant progression in that order. This study investigates how transcriptional aberrations in adenocarcinoma cells at the early stage define the clinical phenotypes of adenocarcinoma tumors at the advanced stage.

Experimental Design: We comprehensively searched for differentially expressed genes between preinvasive and invasive cancer cells in one minimally invasive adenocarcinoma using laser capture microdissection and DNA microarrays. We screened expression of candidate genes in 11 minimally invasive adenocarcinomas by reverse transcriptase PCR and examined their involvement in preinvasive-to-invasive progression by transfection studies. We then immunohistochemically investigated the presence of candidate molecules in 64 samples of advanced adenocarcinoma and statistically analyzed the findings, together with clinicopathologic variables.

Results: The transcription factors *Notch2* and *Six1* were upregulated in invasive cancer cells in all 11 minimally invasive adenocarcinomas. Exogenous Notch2 transactivated *Six1* followed by *Smad3*, *Smad4*, and *vimentin*, and enlarged the nuclei of NCI-H441 lung epithelial cells. Immunochemical staining for the transcription factors was double positive in the invasive, but not in the lepidic growth component of a third of advanced Ads, and the disease-free survival rates were lower in such tumors.

Conclusions: Paired upregulation of *Notch2* and *Six1* is a transcriptional aberration that contributes to preinvasive-to-invasive adenocarcinoma progression by inducing epithelial–mesenchymal transition and nuclear atypia. This aberration persisted in a considerable subset of advanced adenocarcinoma and conferred a more malignant phenotype on the subset. *Clin Cancer Res; 18(4); 945–55. ©2011 AACR.*

Introduction

Adenocarcinoma is the most widespread histologic subtype of lung cancer in most countries, accounting for almost half of all lung cancers (1). Lung adenocarcinomas, especially advanced tumors, rarely comprise a single histologic component, and more than 90% of lung adenocarcinomas are of the mixed subtype according to the 2004 WHO classification (2). In an effort to address the complex histologic heterogeneity of adenocarcinomas, a new classification has recently been proposed (3). According to it, a small tumor with the lepidic growth pattern is diagnosed as either adenocarcinoma *in situ* or minimally invasive adenocarcinoma, depending on the presence or absence of microinvasion ($\leq$ 5 mm). If a microinvasion focus of a minimally invasive adenocarcinoma becomes overt (overt invasion; > 5mm), the tumor will be then diagnosed as lepidic-predominant invasive adenocarcinoma. As might be predicted from these diagnostic criteria, to clearly distinguish between adenocarcinoma *in situ* and minimally invasive adenocarcinoma, as well as between minimally invasive adenocarcinoma and lepidic-predominant invasive adenocarcinoma can be difficult. Rather, it seems reasonable to consider that a significant subset of these 3 subtypes is biologically serial and that each subtype represents a different stage of adenocarcinoma progression.

The concept of progression from adenocarcinoma *in situ* to minimally invasive adenocarcinoma is widely accepted (4–9). Noguchi and colleagues noted 2 types of small

Authors' Affiliations: [1]Surgical Oncology, Division of Genome Radiobiology and Medicine, Programs for Biomedical Research, Graduate School of Biomedical Sciences, Hiroshima University, Hiroshima; [2]Division of Molecular Pathology, Institute of Medical Science, University of Tokyo, Tokyo; and [3]Department of Pathology, Faculty of Medicine, Kinki University, Osaka, Japan

Note: Supplementary data for this article are available at Clinical Cancer Research Online (http://clincancerres.aacrjournals.org/).

Corresponding Author: Akihiko Ito, Department of Pathology, Faculty of Medicine, Kinki University, 377-2 Ohno-Higashi, Osaka-Sayama, Osaka 589-8511, Japan. Phone: 81-72-366-0221; Fax: 81-72-360-2028; E-mail: aito@med.kindai.ac.jp

doi: 10.1158/1078-0432.CCR-11-1946

Published OnlineFirst December 21, 2011; DOI:10.1158/1078-0432.CCR-11-1946

Translational Relevance

Lung adenocarcinomas with mainly lepidic growth component are diagnosed as *in situ*, minimally invasive adenocarcinoma, or lepidic-predominant invasive adenocarcinoma types, depending on the size of invasive foci. In a minimally invasive adenocarcinoma, differentially expressed genes were comprehensively searched between the preinvasive and invasive components, and 2 transcriptional factors, *Notch2* and *Six1*, were identified as genes upregulated in the invasive component in all 11 minimally invasive adenocarcinomas examined. Transfection experiments suggested that Notch2 and Six1 cooperatively induced epithelial–mesenchymal transition of adenocarcinoma cells. Clinicopathologic analyses revealed that upregulation of both Notch2 and Six1 in invasive foci was detected in one-third of 64 lepidic-predominant invasive adenocarcinomas, and these tumors represented an aggressive phenotype. Paired upregulation of *Notch2* and *Six1* seemed to occur during preinvasive-to-invasive adenocarcinoma progression and define a more malignant subset of advanced adenocarcinoma. Notch2 and Six1 are not only useful biomarkers for malignant potential of adenocarcinoma but also can be therapeutic targets in adenocarcinoma.

(maximum diameter, < 2 cm) adenocarcinomas. These are type A (adenocarcinoma *in situ* according to the 2011 classification) that consists entirely of neoplastic cells that grow in lepidic growth pattern and type C (minimally invasive adenocarcinoma according to the 2011 classification) that consists of peripheral lepidic growth and a central microinvasion focus. The 2 types of tumors differ clinicopathologically. (i) After complete resection, patients with type A have 100% disease-specific survival, whereas the 5-year survival rate for patients with type C is 75% (9). (ii) Type C tumors have higher rates of p53 positivity, proliferation, and nuclear atypia than type A (8, 10, 11). Interpreting these data based on the 2011 classification, the microinvasion focus of minimally invasive adenocarcinoma is considered to develop due to the malignant progression of noninvasive, *in situ* neoplastic cells of the lepidic growth component. In contrast to the development of type C or minimally invasive adenocarcinoma tumors, the progression of minimally invasive adenocarcinoma to more advanced forms, including lepidic-predominant invasive adenocarcinoma, has not been studied in detail.

Genetic studies of adenocarcinoma progression have found mutations in *KRAS* and *EGFR* at the preinvasive stage, such as atypical adenomatous hyperplasia and adenocarcinoma *in situ* (12–15), and some adenocarcinomas have the amplification of these genes at the later stage of invasion and metastasis (7, 16, 17). Besides such genomic alterations, specific transcriptional pathways seem to become upregulated during the progression of adenocarcinoma, because recent findings have increasingly clarified that lung cancer progression is promoted by epithelial–mesenchymal transition (EMT; ref. 18) that is controlled by a group of transcription factors that includes Slug, which is a zinc finger type (19). The homeobox transcription factors Oct4 and downstream Nanog both function upstream of Slug to promote EMT in A549 lung adenocarcinoma cells (20). Although lung adenocarcinoma progression is assumed to be a stepwise process triggered by multiple genetic aberrations, which aberration(s) accounts for each process in the stepwise progression requires precise examination.

In this study, we attempted to obtain the genetic evidence, indicating that all or a subset of lepidic-predominant invasive adenocarcinoma develops from minimally invasive adenocarcinoma, and to clarify what clinical phenotypes the subset has. For this purpose, we designed the experiments that were composed of 3 parts. In the first part, we aimed to comprehensively compare the gene expression profiles between lepidic growth and microinvasion cancer cells from a single minimally invasive adenocarcinoma and successfully identified 2 transcription factors *Notch2* and *Six1* as genes upregulated in microinvasion cells. In the second part, we examined whether the identified genes might play causative roles in early-stage adenocarcinoma progression from lepidic growth to microinvasion cells, and found that Notch2 and Six1 coordinately induced EMT and nuclear atypia in lung epithelial cells. Finally in the third part, we immunohistochemically stained 64 specimens of lepidic-predominant invasive adenocarcinoma for Notch2 and Six1 and found that a third were a simple advanced form of minimally invasive adenocarcinoma, judging from the upregulation of Notch2 and Six1 in overt invasion cells. Importantly, the disease-free survival of patients with such tumors was poorer.

Materials and Methods

Sample selection

This study included patients with both consolidated lung tumors and ground glass opacities on chest high-resolution computed tomography images who underwent lobectomy or segmentectomy at Hiroshima University Hospital between 2007 and 2010 (Hiroshima, Japan). All patients provided written, informed consent to participate in this study and our Institutional Review Board approved the protocol (approval number: Hi-29). Half of the cancerous tissues were placed in Ultramount Aqueous Permanent Mounting Medium (DakoCytomation) and frozen for later studies, whereas the other half was preserved in 10% formalin for diagnosis. Gene expression was analyzed in samples of minimally invasive adenocarcinoma from 11 patients and 64 lepidic-predominant invasive adenocarcinoma tumor samples were immunohistochemically stained.

Cell culture

NCI-H441 human lung papillary adenocarcinoma cells, A549 human lung adenocarcinoma cells and MDA-MB-231

Published OnlineFirst December 21, 2011; DOI:10.1158/1078-0432.CCR-11-1946

human breast cancer cells were purchased from the American Type Culture Collection and RERF-LC-MS human lung adenocarcinoma cells were from Japanese Cancer Research Resources Bank (JCRB, Osaka, Japan) in 2010, and all experimentation using cell lines proceeded within 6 months after resuscitation. NCI-H441 cells and A549 cells were grown in RPMI-1640 (Nacalai Tesque) and Dulbecco's Modified Eagle Medium (Nacalai Tesque) supplemented with 10% FBS, antibiotics containing 100 units/mL penicillin, 100 μg/mL streptomycin (Invitrogen), and 0.01M-HEPES buffer (Nacalai Tesque) at 37°C in 5% CO_2/95% air. RERF-LC-MS cells were grown in Eagle's minimal essential medium (Nacalai Tesque) supplemented with 10% FBS, antibiotics, and 0.1 mmol/L nonessential amino acids (GIBCO-Invitrogen) at 37°C in 5% CO_2/95% air. MDA-MB-231 cells were grown in L-15 (Sigma-Aldrich) medium supplemented with 10% FBS, antibiotics, and 0.3 g/L L-glutamine (Sigma-Aldrich) at 37°C in 100% air.

Laser capture microdissection

Serial 15-μm sections of the 11 frozen minimally invasive adenocarcinoma tumors were stained with hematoxylin. Only cancer cells were selectively and separately collected from the lepidic growth and microinvasion components using laser capture microdissection (LMD7000; Leica Microsystems GmbH). The cancer cells were placed in the caps of collection tubes containing Tris [2-carboxyethyl] phosphine hydrochloride buffer. The collection time for one slide was 30 minutes. Twenty slides were done for each component. Each cell pool was frozen with dry ice immediately after collection.

RNA purification and amplification with Cy3 or Cy5 labeling

Total RNA was extracted from each cell pool using NucleoSpin RNA XS (Macherey-Nagel GmbH & Co. KG) and from one small (≤ 1 cm) minimally invasive adenocarcinoma tumor and then cDNAs and amino allyl aRNA were synthesized from the RNA using Amino Allyl MessageAmp II aRNA Amplification Kits (Applied Biosystems). CyeDye coupling and fragmentation proceeded according to a protocol supplied by Toray Industries Inc. The concentration, purity, and integrity of the amplified and labeled aRNA were determined using a Eukaryotes Total RNA Nano Series II (Agilent Technologies). Total RNA from cultured cells was also extracted using NucleoSpin RNA XS.

Gene microarray analysis

Amplified RNA samples from microinvasion components were analyzed using 3D-Gene Human Oligo chip 25k (Toray Industries Inc.) microarrays of 25,370 distinct genes and RNA samples from lepidic growth components as controls. The 3-dimensional microarrays were constructed with wells as spaces between probes and cylinder stems with 70-mer oligonucleotide probes on the top to promote efficient hybridization. Cy3- or Cy5-labeled aRNA pools in hybridization buffer were hybridized for 16 hours according to the supplier's protocol (www.3d-gene.com). Hybridization signals were scanned using ScanArray Express Scanner (PerkinElmer) and processed using GenePixPro version 5.0 (Molecular Devices). Signals detected for each gene were normalized by global normalization (Cy3/Cy5 ratio median = 1) and Cy3/Cy5 normalized ratios >2.0 or <0.5 were, respectively, defined as commonly upregulated or downregulated genes.

Semiquantitative reverse transcriptase PCR

We analyzed the expression of *Notch2*, *Six1*, *thyroid transcription factor-1* (*TTF-1*), *Smad3*, *Smad4*, *vimentin*, *E-cadherin*, and *GAPDH* mRNA using reverse transcriptase PCR (RT-PCR) using SuperScriptTMIII First-Strand Synthesis SuperMix (Invitrogen) for the RT. In brief, total RNA was incubated with 50 ng of random hexamer primers and 1 μL of annealing buffer at 65°C for 5 minutes. The RNA was then incubated at 25°C for 5 minutes and at 50°C for 50 minutes in a final volume of 20 μL of reaction mixture containing 1× first-strand reaction mix comprising 5 mmol/L $MgCl_2$, 0.5 mmol/L of each deoxynucleotide triphosphate (dNTP), and 2 μL of SuperScriptTMIII/RNaseOUTTM Enzyme Mix.

The cDNA constructs were amplified by PCR using TaKaRa Ex Taq (Takara). The PCR conditions were 35 cycles of 30 seconds at 94°C (denaturation), 30 seconds at 55°C (annealing), and 30 seconds at 72°C (extension). The sense and antisense primers were 5′-AAAAATGGGGCCAACCGAGAC-3′ and 5′-TTCATCCAGAAGGCGCACAA-3′ for human *Notch2*, 5′-ACTCTCTGCTCGGCCCCCTC-3′ and 5′-AAGGCTGCTGAAACAGGCGT-3′ for human *Six1*, 5′-ATGTCGATGAGTCCAAAG-3′ and 5′-TCACCAGGTCCGA-3′ for human *TTF-1*, 5′-CGGGCCATGGAGCTGTGTGA-3′ and 5′-ACCTGCGTCCATGCTGTGGT-3′ for human *Smad3*, 5′-TCAGGGCCTCAGCCAGGACA-3′ and 5′-TCTCCTCCAGAAGGGTCCACGT-3′ for human *Smad4*, 5′-CAAGGGCCAAGGCAAGTCGC-3′ and 5′-GCCGTGAGGTCAGGCTTGGA-3′ for human *vimentin*, 5′-CCCTGGCTTTGACGCCGAGA-3′ and 5′-AAACGGAGGCCTGATGGGGC-3′ for human *E-cadherin*, and 5′-ACCACAGTCCATGCCATCAC-3′ and 5′-TCCACCACCCTGTTGCTGTA-3′ for human *GAPDH*, respectively. The PCR products were resolved by electrophoresis on 1% agarose gels, stained with ethidium bromide, and densitometrically analyzed. The RT-PCR signal intensity was quantified using ImageJ software (NIH) to compare *Notch2*, *Six1*, *TTF-1*, *Smad3*, *Smad4*, *vimentin*, *E-cadherin*, and *GAPDH* mRNA levels.

Construction of plasmid vectors expressing Notch2 intracellular domain, TTF-1, and siRNA against Six1

The cDNA construct for Notch2 intracellular domain (ICD; amino acids 1,703–2,475) inserts was amplified by PCR using KOD FX DNA polymerase (Toyobo Co. Ltd.) with following primer set: sense, 5′-CCGGATCCATGAAGCGTAAG-3′ (containing the first codon of Notch2 ICD); antisense, 5′-CCGTTAACTCACGCATAAACCTG-3′ (containing the stop codon of Notch2 ICD). The *TTF-1* gene produces 2 alternative transcripts, of which the short form consists of more than 90% of the total transcripts (21). The open reading frame of the short form of the cDNA from

Published OnlineFirst December 21, 2011; DOI:10.1158/1078-0432.CCR-11-1946

NCI-H441 cells was amplified by PCR using the primer set: sense, 5′-CCGAATTCATGTCGATGAGTCCAAAG-3′; antisense, 5′-CCGTTAACTCACCAGGT-CCGA-3′. The PCR products were resolved by electrophoresis on 1% agarose gels and stained with ethidium bromide. Targeted bands were excised from gels and DNA was extracted and purified using the Wizard SV Gel and PCR Clean-Up System (Promega Corporation), as described by the manufacturer. Extracted DNA chains were annealed and ligated into the *Bam*HI/*Hpa*I (for Notch2) and *Eco*RI/*Hpa*I (for TTF-1) sites of pCX4-bsr, a modified pCX-bsr retroviral vector (22) provided by Dr. T. Akagi (Osaka Bioscience Institute, Osaka, Japan), and sequenced.

The pSilencer4.1-CMVneo siRNA plasmid vector (Ambion) was used to construct pSilencer4.1-CMVneo-si-Six1 and the negative control, pSilencer4.1-CMVneo-scramble. A DNA chain with the following sense and antisense sequences was synthesized to target the Six1 sequence: 5′-GATCCCCAGCTCAGAAGAGGAATTTTC-AAGAGAAA-TTCCTCTTCTGAGCTGGTT-3′ (sense) and 5′-AGCTTAACCAGCTCAGAAGAGGAATT-TCTCTTGAA-AATTCCTCTTCTGAGCTGGG-3′ (antisense). The target sequence of the negative control (scramble-pSilencer4.1-CMVneo) was 5′-GATCCCGT-CGATTTTGTGATGCTCG-TCAGTTCAAGAGACTGACGAGCATCACAAAATCGACG-G-TT-3′ (sense) and 5′-AGCTTAACGTCGATTTTGTGA-TGCTCGTCAGTCTCTTGAACTGA-CGAGCATCACAAAAT-CGACGG-3′ (antisense), which has no homology with any human DNA. The DNA chains were annealed and ligated into the *Bam*HI/*Hin*dIII sites of pSilencer4.1-CMVneo to generate pSilencer4.1-CMVneo-si-Six1. The negative control pSilencer4.1-CMVneo-scramble vector was constructed in the same manner. The plasmids were extracted and the accuracy of the constructs was confirmed by sequencing.

Transfection

NCI-H441 cells were transiently transfected with empty pCX4-bsr, pCX4-bsr-Notch2 ICD, or pCX4-bsr-TTF-1 using FuGENE 6 (Roche Applied Science). In brief, 2.0×10^5 cells were seeded on 60-mm culture dishes overnight until 50% to 80% confluence was reached. Serum-free medium (194 μL) and 6.0 μL of FuGENE 6 reagent were mixed in 1.5-mL tubes and incubated for 5 minutes at room temperature. Plasmid vectors (2.0 μg each) were added and the contents were mixed and incubated with transfection reagent and DNA complex for at least 15 minutes at room temperature. The transfection reagent and DNA complex were added drop wise to the cultured cells and incubated for 48 hours. The medium was removed and the cells were rinsed 3 times with PBS. The transfected cells were then used in various experiments. A549, RERF-LC-MS, and MDA-MB-231 were also transiently transfected with empty pCX4-bsr or pCX4-bsr-Notch2 ICD using FuGENE 6.

Double transfection proceeded as follows. NCI-H441 cells were transiently transfected with 2.0 μg of each of pCX4-bsr-Notch2 ICD and the empty pSilencer4.1-CMVneo, or pSilencer4.1-CMVneo-scramble, or pSilencer4.1-CMVneo -si-Six1 using FuGENE 6.

Immunohistochemistry

Tissues fixed with 10% formalin were embedded in paraffin and cut into 4-μm thick sections that were deparaffinized, rehydrated, and autoclaved for 20 minutes at 121°C in 10 mmol/L citrate buffer (pH 6.0) and then incubated in methanol containing 3% peroxide for 5 minutes. The sections were washed 3 times with PBS between all steps of the procedure. Nonspecific Ig binding in the sections was blocked by incubation with PBS containing 2% bovine serum albumin (BSA) for 10 minutes. The sections were then incubated with anti-Notch2 antibody (ab8926, 1:400 dilution; Abcam) and/or anti-Six1 antibody (HPA001893, 1:100 dilution; Sigma-Aldrich) in PBS containing 2% BSA for 2 hours at room temperature, followed by horseradish peroxidase–conjugated anti-rabbit Ig G antibody (1:100 dilution; Santa Cruz) in PBS containing 2% BSA for 2 hours at 4°C. Color was developed using aminoethylcarbazole (DAB; Dako) as the substrate for peroxidase. Tissues were counterstained with hematoxylin and mounted. Negative immunohistochemical control procedures comprised the omission and replacement of primary antibodies with appropriate concentrations of normal rabbit or mouse IgG. Slides were examined using a light microscope (BX51; Olympus) equipped with a CCD camera DP72 (Olympus). The results on the control slides were negative.

Cancer cells were deemed positive for Notch2 when the cytoplasm of over half of the cancer cells in each of the lepidic growth and microinvasion components was intensely stained. Other staining profiles were defined as negative. Cancer cells were deemed positive for Six1 when nuclei in over half of the cancer cells in each of the lepidic growth and microinvasion components were intensely stained. Other staining profiles were defined as negative.

Nuclear size analysis

Five minimally invasive adenocarcinoma tumors that contained a Notch2-negative lepidic growth component and a Notch2-positive microinvasion component were immunohistochemically selected. The greatest nuclear dimension of cancer cells in both the lepidic growth and microinvasion components was separately determined in 5 tumors using hematoxylin and eosin (H&E) staining and light microscopy (BX51). The greatest nuclear dimension of 200 cells was measured in random fields for each component from each tumor. The greatest nuclear dimension of the control and of NCI-H441 cells transfected *in vitro* with empty pCX4-bsr, pCX4-bsr-Notch2 ICD, or pCX4-bsr-TTF-1 was assessed by nuclear staining using 4′,6-diamino-2-phenylindole (DAPI) and the fluorescence microscope, Axio Observer D1 (Carl Zeiss). We determined the nuclear dimensions of 100 cells in randomly selected fields in 3 independent experiments.

Statistical analysis

Data about signal intensity and cell morphology are described as means ± SD or as means ± SE and were analyzed using Student *t* test. The clinicopathologic findings were analyzed using the Mann–Whitney *U* test for

Published OnlineFirst December 21, 2011; DOI:10.1158/1078-0432.CCR-11-1946

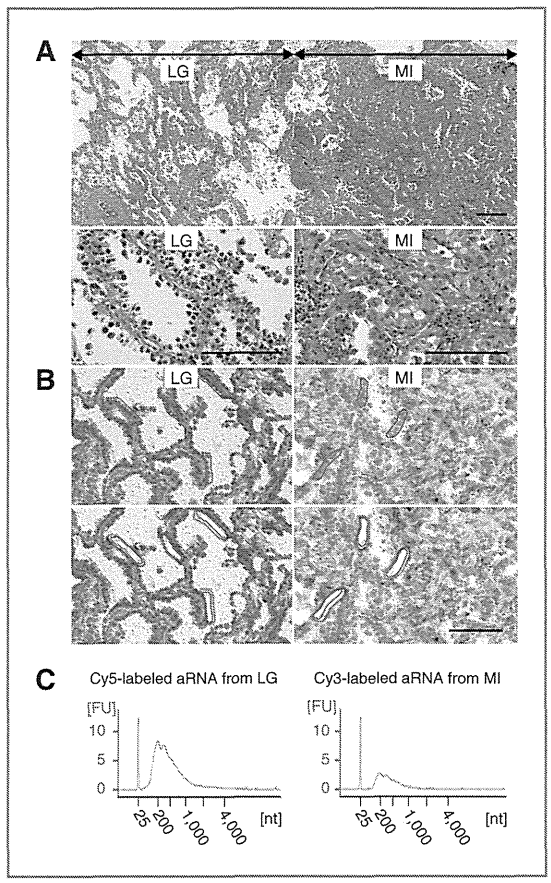

Figure 1. Laser capture microdissection of lepidic growth (LG) and microinvasion (MI) cancer cells from a single minimally invasive adenocarcinoma (case 1) and probe preparation for DNA microarray analysis. A, photomicrograph of minimally invasive adenocarcinoma from case 1 stained with H&E. Top, low-power field view (original magnification, ×100) containing both lepidic growth and microinvasion components; bottom, high-power field view (original magnification, ×400) of each component. B, lepidic growth and microinvasion cancer cells collected by laser capture microdissection from frozen sections of minimally invasive adenocarcinoma tumor. Cancer cells circled in red (top) were cut out using laser pulses run along the circles (bottom). C, verification of aRNA probes for DNA microarray analysis. Total RNA extracted from pools of lepidic growth and microinvasion cancer cells served as templates for preparation of aRNA probes. Quality and quantities of probes were verified by resolving Cy3- or Cy5-labeled aRNA by capillary gel electrophoresis. The amounts of RNA extracted and amplified were 46.2 ng and 14.3 μg for lepidic growth component and 48.4 ng and 4.0 μg for microinvasion component, respectively. Bar, 100 μm.

continuous variables and χ^2 tests for categorical variables. Disease-free survival (DFS) curves were calculated using the Kaplan–Meier method. Univariate and multivariate analyses were done using the log-rank and logistic regression tests, respectively. A P value of ≤ 0.05 was regarded as significant.

Results

Isolation of genes that are differentially expressed in lepidic growth and microinvasion cancer cells in a single minimally invasive adenocarcinoma

A small (1 cm in greatest dimension), solitary lung tumor was surgically resected and histopathologically diagnosed as minimally invasive adenocarcinoma (formerly, type C by Noguchi classification; Fig. 1A; case 1 in Fig. 2A and Supplementary Table S1). We separately isolated lepidic growth and microinvasion cancer cells without contamination from frozen tumor sections using a laser capture microdissection system (Fig. 1B). We extracted total RNAs from about 500 lepidic growth and microinvasion cancer cells and then amplified and labeled the RNAs using T7 RNA polymerase. Fig. 1C shows the amounts and quality of the original total RNAs and amplified aRNAs. The aRNAs were comparatively analyzed using highly sensitive oligo DNA microarrays. The complete gene expression dataset of the microdissected minimally invasive adenocarcinoma specimen is available at Gene Expression Omnibus (GEO) accession number GSE30663 (23). The numbers of genes whose expression levels were double or more and half or less in the microinvasion cancer cells were 2,905 and 2,143, respectively. Supplementary Table S2 shows the top 30 of each of

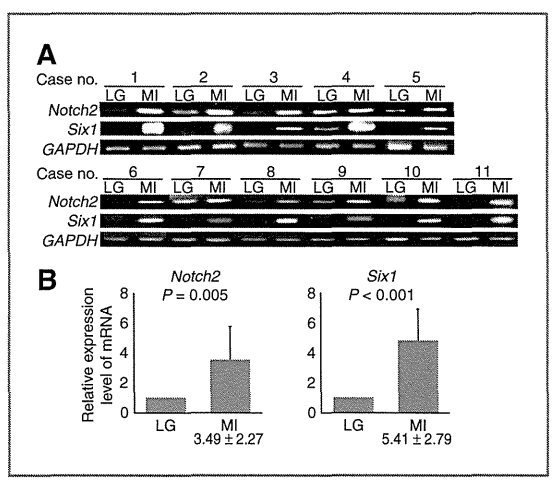

Figure 2. RT-PCR analyses of *Notch2* and *Six1* in total RNA from lepidic growth (LG) and microinvasion (MI) cancer cells in 11 minimally invasive adenocarcinomas. lepidic growth and microinvasion cancer cells were separately collected from frozen sections of minimally invasive adenocarcinomas (cases 1 to 11 listed in Supplementary Table S1) using laser capture microdissection. Total RNAs were extracted from each cell pool and analyzed by RT-PCR using primer sets for *Notch2*, *Six1*, or *GAPDH*. Portions of PCR products were resolved by electrophoresis on 1% agarose gels (A). All band intensities were converted to densitometric values; *Notch2* and *Six1* values were normalized to that of *GAPDH* and then means and SD of 11 minimally invasive adenocarcinomas were calculated. Expression levels of *Notch2* and *Six1* mRNA in microinvasion cancer cells are expressed as relative values normalized to 1 for means in lepidic growth cancer cells (B).

Published OnlineFirst December 21, 2011; DOI:10.1158/1078-0432.CCR-11-1946

the upregulated (>94-fold) and downregulated (<1/25.4-fold) candidate genes.

Upregulation of Notch2 and its downstream Six1 in microinvasion cancer cells

We found that *Six1* (136-fold) was the most upregulated among the top 30 genes in microinvasion cancer cells, and *Notch2* was 10.7-fold upregulated in the complete dataset. We considered that this paired upregulation was worthy of further investigation because both Six1 and Notch2 can function as transcription factors and Six1 is a putative downstream target of Notch2 (24, 25). As with minimally invasive adenocarcinoma from case 1, we extracted total RNAs from lepidic growth and microinvasion cancer cells separately from minimally invasive adenocarcinomas resected from cases 2 to 11 (Fig. 2A and Supplementary Table S1). *Six1* and *Notch2* mRNA expression was then screened in all 11 minimally invasive adenocarcinomas by semiquantitative RT-PCR. Significantly more mRNA for either gene was found in microinvasion than in lepidic growth cancer cells from all 11 minimally invasive adenocarcinomas (Fig. 2A and B). The expression of Notch2 and Six1 proteins was examined in the case 10 minimally invasive adenocarcinoma by immunohistochemistry. Notch2 and Six1 immunoreactive signals were clearly detected in the cytoplasm and nucleus of microinvasion cancer cells, respectively, whereas lepidic growth component cells were nearly completely negative for the two molecules (Fig. 3).

We speculated whether Notch2 upregulation results in *Six1* transactivation in lung epithelial cells and examined this notion in NCI-H441 cells that have been widely studied as lung epithelial cells. The results of RT-PCR analyses revealed that these cells expressed endogenously undetectable levels of *Notch2* or *Six1* (Fig. 4A, lane 1). Because Notch2 is enzymatically processed to release its ICD that functions as a transcription factor (26), we subcloned Notch2 ICD cDNA into the mammalian expression vector, pCX4-bsr. NCI-H441 cells transfected with this plasmid contained not only abundant exogenous transcripts for Notch2 ICD but also abundant endogenous transcripts for Six1 (Fig. 4A, lane 3 and Supplementary Fig. S1). We also transfected NCI-H441 cells with the cDNA for TTF-1, well known as a lung epithelial transcription factor, but *Six1* transactivation was undetectable (Fig. 4A, lane 4 and Supplementary Fig. S1). Similar experiments using MDA-MB-231 breast cancer cells that express endogenously detectable levels of *Notch2* and *Six1* showed that exogenous Notch2 ICD did not upregulate, but rather slightly downregulated *Six1* (Fig. 4A, lanes 8–10). These results suggested that Notch2 specifically transactivates *Six1* in NCI-H441.

Involvement of Notch2 and Six1 in EMT and nuclear atypism in lung epithelial cells

Notch2 and Six1 promote EMT in various cancers partly through activating the TGF-β intracellular signaling pathways that involve the intracellular signal transducers Smad3 and Smad4 (27–29). Consistent with their epithelioid morphology, NCI-H441 cells expressed easily and faintly detectable levels of *E-cadherin* and *vimentin*, respectively (Fig. 4A, lane 1). The expression levels of these two genes were inverse in NCI-H441 cells transfected with Notch2 ICD cDNA (Fig. 4A, lane 3 and Supplementary Fig. S2). Such transfection also resulted in *Smad3* and *Smad4* transactivation (Fig. 4A, lane 3 and Supplementary Fig. S2). Transfection with the empty vector did not alter the endogenous expression of these 4 genes (Fig. 4A, lane 2 and Supplementary Fig. S2). Transfection with TTF-1 resulted in *vimentin* transactivation and *E-cadherin* downregulation (Fig. 4A, lane 4 and Supplementary Fig. S2). Notch2 seemed to promote EMT in NCI-H441 cells more efficiently than TTF-1. NCI-H441 cells were transfected with Notch2 ICD cDNA and with either Six1-targeting siRNA or a control scrambled siRNA. The Six1-targeting siRNA abrogated not only Notch2 ICD–induced transactivation of *Six1* but also

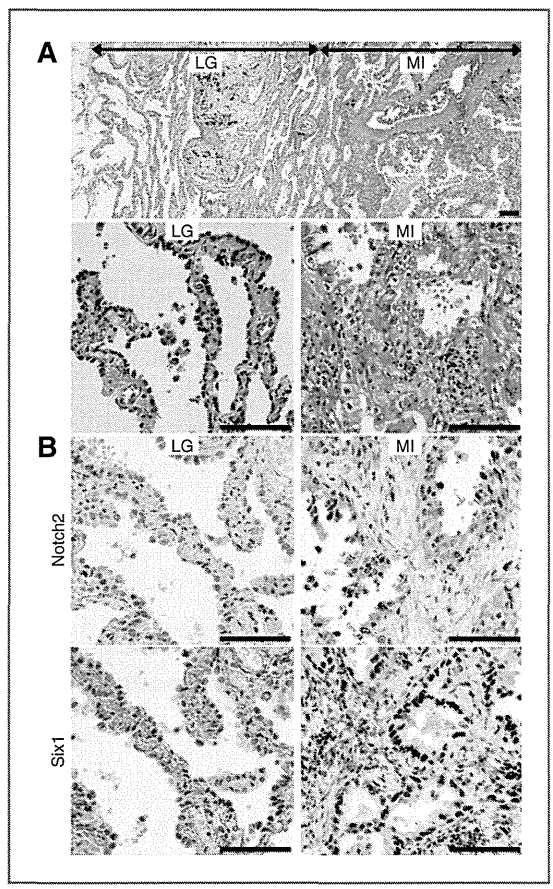

Figure 3. Immunohistochemical staining for Notch2 and Six1 on a minimally invasive adenocarcinoma. Serial sections of the minimally invasive adenocarcinoma from case 10 (listed in Fig. 2A and Supplementary Table S1) were stained with H&E (A) and immunostained with either the Notch2 or Six1 antibody (B). Representative staining images of the lepidic growth (LG) and microinvasion (MI) components are shown in the left and right panels, respectively. Bar, 100 μm.

Published OnlineFirst December 21, 2011; DOI:10.1158/1078-0432.CCR-11-1946

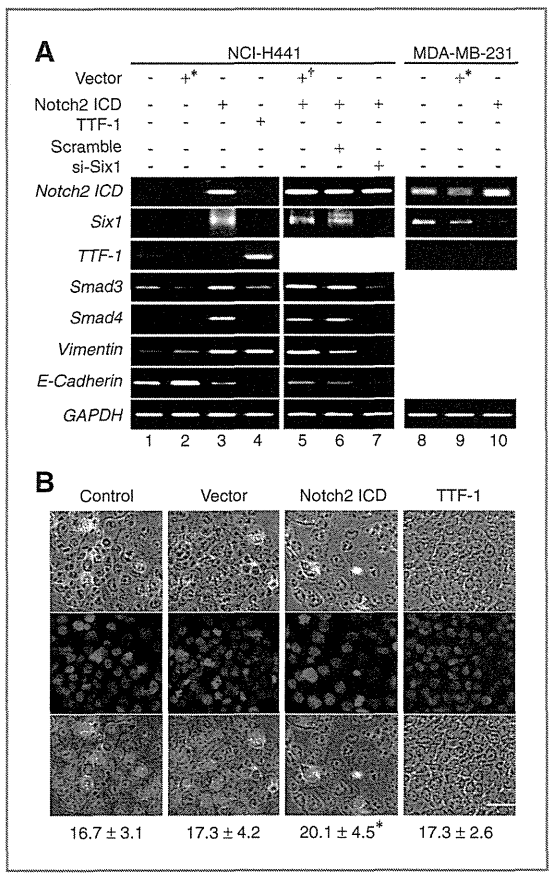

Figure 4. Transcriptional and cell morphologic alterations induced by exogenous Notch2 ICD in NCI-H441 cells. A, expression of EMT-related genes in NCI-H441 and MDA-MB-231 cells before and after transfection with various transcription factors and si-RNA. NCI-H441 and MDA-MB-231 cells were transiently transfected with pCX4-bsr empty (*lanes 2 and 9) or with vectors expressing either Notch2 ICD (lanes 3 and 10) or TTF-1 (lane 4). NCI-H441 cells were transiently transfected in some experiments with Notch2 ICD cDNA and with either empty pSilencer4.1-CMVneo (†lane 5) or vectors expressing scrambled (lane 6) or Six1-targeting (lane 7) siRNA. Total RNAs extracted from intact or transfected cells were analyzed by RT-PCR using primer set for indicated genes. Portions of PCR products were resolved by electrophoresis on 1% agarose gels. B, changes in sizes of nuclei in NCI-H441 cells transfected with Notch2 ICD cDNA. NCI-H441 cells were transfected or not (control) with either empty pCX4-bsr or vectors expressing cDNAs for Notch2 ICD or TTF-1 and then stained with DAPI to visualize nuclei (blue). Phase-contrast (top) and UV laser (middle) images of cells are merged (bottom). Sizes of nuclei were determined as described in Materials and Methods, and calculated means and SE are shown below the images. *, $P < 0.01$ compared with values of other types of cells. Bar, 50 μm.

that of *Smad3*, *Smad4*, and *vimentin*, whereas it further enhanced the Notch2 ICD–induced downregulation of *E-cadherin* (Fig. 4A, lane 7). Control transfection did not alter the gene expression induced by Notch2 ICD (Fig. 4A, lanes 5 and 6). These results indicated that Six1 is essential for Notch2 to transactivate *Smad3*, *Smad4*, and *vimentin*, but not to downregulate *E-cadherin*.

Notch2 ICD transfection experiments, followed by RT-PCR, were conducted on 2 other lung adenocarcinoma cell lines, A549 and RERF-LC-MS, both of which expressed endogenously undetectable levels of Notch2 and Six1 (Supplementary Fig. S3). Exogenous Notch2 ICD in these cells induced gene expression alterations resembling those in NCI-H441 cells, except that *Smad4* and *E-cadherin* were not upregulated in A549 and RERF-LC-MS, respectively (Supplementary Fig. S3). These results suggested that Notch2 and Six1 played pivotal roles in inducing EMT of lung adenocarcinoma cells.

Early-stage lung adenocarcinoma progression is assumed to be associated with an increase in the size of cancer cell nuclei (8). We measured the greatest dimension of cancer cell nuclei in 5 minimally invasive adenocarcinomas and found significantly larger nuclei in micro-invasion, than in lepidic growth cancer cells from all 5 minimally invasive adenocarcinomas (Supplementary Table S1). A comparison between intact NCI-H441 cells and those transfected with the Notch2 ICD cDNA showed significantly larger nuclei in the transfectants than in the intact cells (Fig. 4B). Transfection with empty vector or with TTF-1 cDNA did not alter the size of nuclei in NCI-H441 cells (Fig. 4B).

Upregulation of Notch2 and Six1 defines a clinically aggressive phenotype of lepidic-predominant invasive adenocarcinoma

We immunohistochemically analyzed 64 samples of lepidic-predominant invasive adenocarcinoma tumors using antibodies against Notch2 and Six1. Table 1 summarizes the clinicopathologic features of each case. The immunohistochemical staining results were judged positive when more than 50% of the cancer cells in each of the lepidic growth and overt invasion components had significant cytoplasmic (Notch2) or nuclear (Six1) staining. The tumors were classified based this judgment as double (Notch2 and Six1) negative in lepidic growth, but double positive in overt invasion (N/P; $n = 23$) cells; double negative in both components (N/N; $n = 19$); double positive in both components (P/P; $n = 19$) and other ($n = 3$; summarized in Table 1). A representative staining profile of N/P tumors was shown in Supplementary Fig. S4. A statistical analysis of the clinicopathologic parameters among the groups showed that the N/P group was less favorable than the N/N group with respect to pT, pN, PL factor, and ly factor (Table 1). Univariate log-rank analyses of Kaplan–Meier survival curves revealed that DFS duration was shorter in the N/P, than in the N/N group ($P = 0.015$; Fig. 5). DFS duration was also affected by various clinicopathologic parameters including pStage, pT, pN, PL factor, and ly factor (Supplementary Table S3). Multivariate logistic regression analyses among the 3 groups revealed that the N/P and P/P groups were more likely to recur than the N/N group in 2-year post-operative follow-up (Supplementary Table S4).

Published OnlineFirst December 21, 2011; DOI:10.1158/1078-0432.CCR-11-1946

Table 1. Classification of patients with lepidic-predominant invasive adenocarcinoma according to Notch2 and Six1 immunohistochemical findings

		Notch2 and Six1					
Variable	**All patients**	**N/N**	**N/P**	**P/P**	**Other**		***P***
Sex						N/N vs. N/P	0.59
Male	36	10	14	11	1	N/N vs. P/P	0.74
Female	28	9	9	8	2	N/P vs. P/P	0.85
Age						N/N vs. N/P	0.95
Mean	71	70.5	70.7	70.8	78.3	N/N vs. P/P	0.93
Range	49–86	49–86	58–83	56–85	74–85	N/P vs. P/P	0.97
pStage[a]						N/N vs. N/P	0.33
IA + IB	52	17	18	14	3	N/N vs. P/P	0.21
IIA + IIB + IIIA + IIIB	12	2	5	5	0	N/P vs. P/P	0.73
pT[a]						N/N vs. N/P	0.04
1a + 1b	39	15	11	11	2	N/N vs. P/P	0.16
2a + 2b + 3	25	4	12	8	1	N/P vs. P/P	0.52
pN[a]						N/N vs. N/P	0.03
0	55	19	18	15	3	N/N vs. P/P	0.03
1 + 2	9	0	5	4	0	N/P vs. P/P	0.96
PL factor[a]						N/N vs. N/P	0.005
0	50	18	13	17	2	N/N vs. P/P	0.55
≥1	14	1	10	2	1	N/P vs. P/P	0.02
ly Factor[a]						N/N vs. N/P	0.039
0	46	18	16	10	2	N/N vs. P/P	0.003
1	18	1	7	9	1	N/P vs. P/P	0.26
v Factor[a]						N/N vs. N/P	0.67
0	56	18	21	14	3	N/N vs. P/P	0.08
1	8	1	2	5	0	N/P vs. P/P	0.13
Tumor size (mm)						N/N vs. N/P	0.89
Mean	25.3	25.5	25	24.7	30	N/N vs. P/P	0.82
Range	11–70	11–70	15–40	12–38	15–50	N/P vs. P/P	0.87

[a]According to TNM classification (7th Edition).

Discussion

This study comprised 3 parts. A clinical issue had to be considered for the first part that compared comprehensive gene expression between lepidic growth and microinvasion cancer cells in individual minimally invasive adenocarcinomas. Because the cut surface at the greatest dimension of the tumor is used for pathologic diagnosis, remaining specimens for LMD contained only a small amount of each component, particularly the microinvasion component. The original estimated amount of total RNA used for the present DNA microarray analysis was in the order of 100 ng per component or less. This limitation might have caused considerable RNA degradation and consequently resulting in shorter aRNA probes (theoretical average length, ~1.5 kb) (Fig. 1C). Regardless, the DNA microarray analysis seemed reliable because (i) the range of the relative expression levels of 10 housekeeping genes was sufficiently small

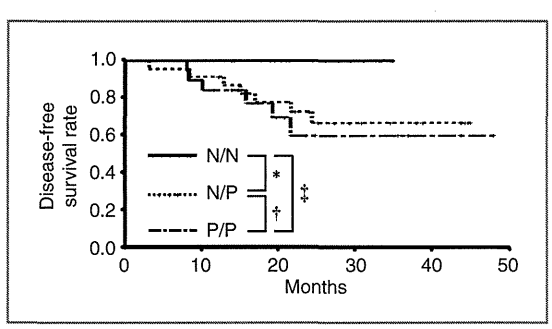

Figure 5. DFS rates of 64 lepidic-predominant invasive adenocarcinomas grouped by Notch2 and Six1 immunohistochemistry. DFS rates of N/N, N/P, and P/P tumor groups shown as function of months. The mean interval of DFS (95% CI) for N/P and P/P are 34.9 (28.8–41.1) months and 34.7 (26.2–43.2) months, respectively. Values for N/N were not calculated because N/N tumors did not recur. *, $P = 0.015$; †, $P = 0.626$; ‡, $P = 0.006$.

Published OnlineFirst December 21, 2011; DOI:10.1158/1078-0432.CCR-11-1946

(within 0.5- to 2-fold) between lepidic growth and microinvasion cells (Supplementary Table S2), and (ii) differential expression of the selected 2 genes, that is, *Notch2* and *Six1* genes, was reproducibly confirmed by RT-PCR (Fig. 2A, case 1). These results indicate that tumor lesions at the early stage that contain cancer cells with different malignant potential, for example, *in situ* and invasive cells in minimally invasive adenocarcinoma, are practical for comparative gene expression analyses among cancer cells during progression *in vivo*.

Both *Notch2* and *Six1* were upregulated in microinvasion cancer cells not only in the minimally invasive adenocarcinoma that was analyzed using DNA microarrays but also in 10 other minimally invasive adenocarcinomas examined. We therefore considered that paired upregulation of Notch2 and Six1 is commonly associated with the progression of lepidic growth to microinvasion cancer cells in minimally invasive adenocarcinoma. Notch2 is a cell membrane–bound ligand-dependent receptor for the Type 1 transmembrane protein family named Notch (30–33). When Notch ligands bind to Notch2 receptors between two neighboring cells, Notch2 is cleaved through a cascade of proteolytic enzymes, including γ-secretase, and released Notch2 ICD translocates into the nucleus where it transcriptionally activates Notch2 target genes (26). Although Notch1 and Notch3, other members of the Notch family, have long been regarded as candidate molecules responsible for the development of lung cancer (34–36), whether Notch2 has similar roles remains to be determined. Six1 is a homeodomain transcription factor (37) and a putative downstream target of Notch2 (24, 25). Interestingly, Ford and colleagues showed that Six1 stimulates the malignant transformation of mammary epithelial cells through transactivating *cyclin A1* (38, 39) and induces EMT in mammary cancer cells through the induction of TGF-β signaling (27, 40). These findings suggested that Notch2 and Six1 play coordinate roles during the early-stage lung adenocarcinoma progression.

The second part of this study examined this notion using transfection experiments. Consistent with previous characterization, exogenous expression of the Notch2 ICD resulted in *Six1* transactivation in NCI-H441 lung epithelial cells. The exogenous Notch2 ICD also transactivated *Smad3*, *Smad4*, and *vimentin* in association with the downregulation of *E-cadherin*. Similar transactivation effects of Notch2 ICD were detected in 2 other types of epithelial cells derived from lung adenocarcinomas. Interestingly, Six1 was notably essential for transactivation of the 3 genes, but not for the downregulation of *E-cadherin*, suggesting that Notch2 and Six1 coordinately played a causative role in inducing EMT during the progression of lepidic growth to microinvasion cells. Exogenous expression of the Notch2 ICD in NCI-H441 cells also resulted in nuclei becoming enlarged. This was in accordance with the cytologic finding that nuclei were larger in microinvasion cancer cells than in lepidic growth cells from 5 minimally invasive adenocarcinomas examined. These results supported the notion that the transcriptional cascades activated coordinately by Notch2 and Six1 are involved in lepidic growth-to-microinvasion progression.

The third part of the study immunohistochemically investigated Notch2 and Six1 in 64 samples of lepidic-predominant invasive adenocarcinoma tumors and found that they could be assigned almost equally into groups on the basis of positive and negative staining as N/N, N/P, and P/P. Consistent with the results of the second part of the study showing that Six1 is a downstream target of Notch2, these transcription factors were either double negative or double positive in lepidic growth and overt invasion cancer cells, respectively, with some exceptions. As might be predicted from the diagnostic criteria, lepidic-predominant invasive adenocarcinoma seemed to include heterogeneous tumors with distinct natural histories and genetic alterations. Judging from the immunostaining profiles of lepidic growth and overt invasion cells, N/P tumors seem to be a simple advanced form of minimally invasive adenocarcinoma, in which microinvasion cells have grown into an overt invasion focus, and N/N tumors develop via other molecular mechanisms than those involving Notch2 and Six1. On the other hand, the origin of P/P tumors is uncertain, but they might be a more advanced form of N/P tumors. Because lepidic growth cancer cells were positive for both Notch2 and Six1, they might be potentially invasive. This speculation is reminiscent of a recent report by Anami and colleagues who notably pointed out that the lepidic growth pattern might represent the intraalveolar epithelial spread of overt invasion cancer cells (41). Whether or not lepidic growth cancer cells are invasive did not seem to affect the prognostic outcomes of patients with lepidic-predominant invasive adenocarcinomas (N/P vs. P/P in Fig. 5). Interestingly, we found that N/N tumors metastasized less often to lymph nodes, were less invasive to lymphatic vessels, and were associated with better DFS than N/P and P/P tumors ($P = 0.015$ and 0.006 by log-rank tests, respectively). These findings agree with a summary of reviews that emphasize the critical role of Notch signals in the malignant progression of non-small cell lung cancer (34–36). The paired upregulation of Notch2 and Six1 seemed to be one transcriptional alteration that is responsible for minimally invasive adenocarcinoma-to-lepidic-predominant invasive adenocarcinoma progression, and it defined a clinically aggressive phenotype subset of lepidic-predominant invasive adenocarcinoma. Because Notch2 and Six1 immunohistochemistry seemed to independently discriminate lepidic-predominant invasive adenocarcinomas with high risk of recurrence in a 2-year postoperative period, during which the recurrence of most lung cancers occurs even after curative-intent therapy (42), it could be a clinically useful examination for selecting patients with lepidic-predominant invasive adenocarcinoma needing intensive follow-up.

Aviel-Ronen and colleagues (2008) examined genomic changes associated with adenocarcinoma *in situ* and minimally invasive adenocarcinoma using array comparative

Published OnlineFirst December 21, 2011; DOI:10.1158/1078-0432.CCR-11-1946

genomic hybridization and found that genomic profiles are indistinguishable between adenocarcinoma *in situ* and minimally invasive adenocarcinoma, although they developed in distinct individuals (5). In contrast, this study successfully revealed that gene expression profiles substantially differed between lepidic growth and microinvasion cancer cells in a single minimally invasive adenocarcinoma. The findings of these two studies and the present results indicate that the Notch2 and Six1 upregulation detected in minimally invasive adenocarcinoma is attributable not to particular genomic alterations, but to environmental factors, including immune and stromal cells around cancer cells. In fact, activation of the Notch2 signaling pathway is cell membrane–bound ligand dependent (26). Although further characterization of lepidic-predominant invasive adenocarcinoma is required at the molecular level, subclassification of lepidic-predominant invasive adenocarcinoma on the basis of Notch2 and Six1 upregulation seems to be clinically important in predicting the prognostic outcomes of patients with lepidic-predominant invasive adenocarcinoma.

Disclosure of Potential Conflicts of Interest

No potential conflicts of interest were disclosed.

Grant Support

This study was supported by grants from the Ministry of Education, Culture, Sports, Science and Technology of Japan and from the Nakatani Foundation of Electronic Measuring Technology Advancement.

The costs of publication of this article were defrayed in part by the payment of page charges. This article must therefore be hereby marked *advertisement* in accordance with 18 U.S.C. Section 1734 solely to indicate this fact.

Received July 28, 2011; revised December 14, 2011; accepted December 16, 2011; published OnlineFirst December 21, 2011.

References

1. Devesa SS, Bray F, Vizcaino AP, Parkin DM. International lung cancer trends by histologic type: male:female differences diminishing and adenocarcinoma rates rising. Int J Cancer 2005;117:294–9.
2. Motoi N, Szoke J, Riely GJ, Seshan VE, Kris MG, Rusch VW, et al. Lung adenocarcinoma: modification of the 2004 WHO mixed subtype to include the major histologic subtype suggests correlations between papillary and micropapillary adenocarcinoma subtypes, EGFR mutations and gene expression analysis. Am J Surg Pathol 2008;32:810–27.
3. Travis WD, Brambilla E, Noguchi M, Nicholson AG, Geisinger KR, Yatabe Y, et al. International association for the study of lung cancer/American Thoracic Society/European Respiratory Society international multidisciplinary classification of lung adenocarcinoma. J Thorac Oncol 2011;6:244–85.
4. Aoyagi Y, Yokose T, Minami Y, Ochiai A, Iijima T, Morishita Y, et al. Accumulation of losses of heterozygosity and multistep carcinogenesis in pulmonary adenocarcinoma. Cancer Res 2001;61:7950–4.
5. Aviel-Ronen S, Coe BP, Lau SK, da Cunha Santos G, Zhu CQ, Strumpf D, et al. Genomic markers for malignant progression in pulmonary adenocarcinoma with bronchioloalveolar features. Proc Natl Acad Sci U S A 2008;105:10155–60.
6. Seki N, Takasu T, Mandai K, Nakata M, Saeki H, Heike Y, et al. Expression of eukaryotic initiation factor 4E in atypical adenomatous hyperplasia and adenocarcinoma of the human peripheral lung. Clin Cancer Res 2002;8:3046–53.
7. Soh J, Toyooka S, Ichihara S, Asano H, Kobayashi N, Suehisa H, et al. Sequential molecular changes during multistage pathogenesis of small peripheral adenocarcinomas of the lung. J Thorac Oncol 2008;3:340–7.
8. Morishita Y, Fukasawa M, Takeuchi M, Inadome Y, Matsuno Y, Noguchi M. Small-sized adenocarcinoma of the lung. Cytologic characteristics and clinical behavior. Cancer 2001;93:124–31.
9. Noguchi M, Morikawa A, Kawasaki M, Matsuno Y, Yamada T, Hirohashi S, et al. Small adenocarcinoma of the lung. Histologic characteristics and prognosis. Cancer 1995;75:2844–52.
10. Maezawa N, Tsuta K, Shibuki Y, Yamazaki S, Maeshima AM, Watanabe S, et al. Cytopathologic factors can predict invasion in small-sized peripheral lung adenocarcinoma with a bronchioloalveolar carcinoma component. Cancer 2006;108:488–93.
11. Terasaki H, Niki T, Matsuno Y, Yamada T, Maeshima A, Asamura H, et al. Lung adenocarcinoma with mixed bronchioloalveolar and invasive components: clinicopathological features, subclassification by extent of invasive foci, and immunohistochemical characterization. Am J Surg Pathol 2003;27:937–51.
12. Lynch TJ, Bell DW, Sordella R, Gurubhagavatula S, Okimoto RA, Brannigan BW, et al. Activating mutations in the epidermal growth factor receptor underlying responsiveness of non-small-cell lung cancer to gefitinib. N Engl J Med 2004;350:2129–39.
13. Paez JG, Janne PA, Lee JC, Tracy S, Greulich H, Gabriel S, et al. EGFR mutations in lung cancer: correlation with clinical response to gefitinib therapy. Science 2004;304:1497–500.
14. Sakamoto H, Shimizu J, Horio Y, Ueda R, Takahashi T, Mitsudomi T, et al. Disproportionate representation of KRAS gene mutation in atypical adenomatous hyperplasia, but even distribution of EGFR gene mutation from preinvasive to invasive adenocarcinomas. J Pathol 2007;212:287–94.
15. Westra WH, Baas IO, Hruban RH, Askin FB, Wilson K, Offerhaus GJ, et al. K-ras oncogene activation in atypical alveolar hyperplasias of the human lung. Cancer Res 1996;56:2224–8.
16. Yatabe Y, Takahashi T, Mitsudomi T. Epidermal growth factor receptor gene amplification is acquired in association with tumor progression of EGFR-mutated lung cancer. Cancer Res 2008;68:2106–11.
17. Tang ZQ, Han LY, Lin HH, Cui J, Jia J, Low BC, et al. Derivation of stable microarray cancer-differentiating signatures using consensus scoring of multiple random sampling and gene-ranking consistency evaluation. Cancer Res 2007;67:9996–10003.
18. Zhang HJ, Wang HY, Zhang HT, Su JM, Zhu J, Wang HB, et al. Transforming growth factor-beta1 promotes lung adenocarcinoma invasion and metastasis by epithelial-to-mesenchymal transition. Mol Cell Biochem 2011;355:309–14.
19. Shih JY, Yang PC. The EMT regulator slug and lung carcinogenesis. Carcinogenesis 2011;32:1299–304.
20. Chiou SH, Wang ML, Chou YT, Chen CJ, Hong CF, Hsieh WJ, et al. Coexpression of Oct4 and Nanog enhances malignancy in lung adenocarcinoma by inducing cancer stem cell-like properties and epithelial-mesenchymal transdifferentiation. Cancer Res 2010;70:10433–44.
21. Li C, Cai J, Pan Q, Minoo P. Two functionally distinct forms of NKX2.1 protein are expressed in the pulmonary epithelium. Biochem Biophys Res Commun 2000;270:462–8.
22. Akagi T, Murata K, Shishido T, Hanafusa H. v-Crk activates the phosphoinositide 3-kinase/AKT pathway by utilizing focal adhesion kinase and H-Ras. Mol Cell Biol 2002;22:7015–23.
23. GEO Browser [Internet]. Bethesda (MD): National Library of Medicine (US); 2002. Expression profiling by array [cited 2011 Jul 14]. Available from: http://www.ncbi.nlm.nih.gov/geo/query/acc.cgi?token=plkbnogawiamexw&acc=GSE30663 Accession Number: GSE30663.

Published OnlineFirst December 21, 2011; DOI:10.1158/1078-0432.CCR-11-1946

24. Bessarab DA, Chong SW, Korzh V. Expression of zebrafish six1 during sensory organ development and myogenesis. Dev Dyn 2004;230: 781–6.
25. Rodriguez S, Sickles HM, Deleonardis C, Alcaraz A, Gridley T, Lin DM. Notch2 is required for maintaining sustentacular cell function in the adult mouse main olfactory epithelium. Dev Biol 2008;314:40–58.
26. Fortini ME. Notch signaling: the core pathway and its posttranslational regulation. Dev Cell 2009;16:633–47.
27. Micalizzi DS, Christensen KL, Jedlicka P, Coletta RD, Baron AE, Harrell JC, et al. The Six1 homeoprotein induces human mammary carcinoma cells to undergo epithelial-mesenchymal transition and metastasis in mice through increasing TGF-beta signaling. J Clin Invest 2009; 119:2678–90.
28. Tang Y, Urs S, Boucher J, Bernaiche T, Venkatesh D, Spicer DB, et al. Notch and transforming growth factor-beta (TGFbeta) signaling pathways cooperatively regulate vascular smooth muscle cell differentiation. J Biol Chem 2010;285:17556–63.
29. Kida Y, Maeda Y, Shiraishi T, Suzuki T, Ogura T. Chick Dach1 interacts with the Smad complex and Sin3a to control AER formation and limb development along the proximodistal axis. Development 2004; 131:4179–87.
30. Grego-Bessa J, Diez J, Timmerman L, de la Pompa JL. Notch and epithelial-mesenchyme transition in development and tumor progression: another turn of the screw. Cell Cycle 2004;3:718–21.
31. Weinmaster G, Roberts VJ, Lemke G. A homolog of *Drosophila* Notch expressed during mammalian development. Development 1991; 113:199–205.
32. Jadhav AP, Mason HA, Cepko CL. Notch 1 inhibits photoreceptor production in the developing mammalian retina. Development 2006; 133:913–23.
33. Artavanis-Tsakonas S, Rand MD, Lake RJ. Notch signaling: cell fate control and signal integration in development. Science 1999;284:770–6.
34. Collins BJ, Kleeberger W, Ball DW. Notch in lung development and lung cancer. Semin Cancer Biol 2004;14:357–64.
35. Konishi J, Kawaguchi KS, Vo H, Haruki N, Gonzalez A, Carbone DP, et al. Gamma-secretase inhibitor prevents Notch3 activation and reduces proliferation in human lung cancers. Cancer Res 2007; 67:8051–7.
36. Ji X, Wang Z, Geamanu A, Sarkar FH, Gupta SV. Inhibition of cell growth and induction of apoptosis in non-small cell lung cancer cells by delta-tocotrienol is associated with Notch-1 down-regulation. J Cell Biochem 2011;112:2773–83.
37. Levine M, Hoey T. Homeobox proteins as sequence-specific transcription factors. Cell 1988;55:537–40.
38. Coletta RD, Christensen K, Reichenberger KJ, Lamb J, Micomonaco D, Huang L, et al. The Six1 homeoprotein stimulates tumorigenesis by reactivation of cyclin A1. Proc Natl Acad Sci U S A 2004;101:6478–83.
39. Coletta RD, Christensen KL, Micalizzi DS, Jedlicka P, Varella-Garcia M, Ford HL. Six1 overexpression in mammary cells induces genomic instability and is sufficient for malignant transformation. Cancer Res 2008;68:2204–13.
40. Farabaugh SM, Micalizzi DS, Jedlicka P, Zhao R, Ford HL. Eya2 is required to mediate the pro-metastatic functions of Six1 via the induction of TGF-beta signaling, epithelial-mesenchymal transition, and cancer stem cell properties. Oncogene 2011; Jun 27 [Epub ahead of print].
41. Anami Y, Iijima T, Suzuki K, Yokota J, Minami Y, Kobayashi H, et al. Bronchioloalveolar carcinoma (lepidic growth) component is a more useful prognostic factor than lymph node metastasis. J Thorac Oncol 2009;4:951–8.
42. Colice GL, Rubins J, Unger MAmerican College of Chest P. Follow-up and surveillance of the lung cancer patient following curative-intent therapy. Chest 2003;123:272S–83S.

Biochemical and Biophysical Research Communications 417 (2012) 462–467

Contents lists available at SciVerse ScienceDirect

Biochemical and Biophysical Research Communications

journal homepage: www.elsevier.com/locate/ybbrc

Tumor suppressor cell adhesion molecule 1 (CADM1) is cleaved by a disintegrin and metalloprotease 10 (ADAM10) and subsequently cleaved by γ-secretase complex

Yusuke Nagara [a], Man Hagiyama [b,c], Naoya Hatano [d], Eugene Futai [a,1], Satoshi Suo [a], Yutaka Takaoka [e], Yoshinori Murakami [b], Akihiko Ito [b,c,*], Shoichi Ishiura [a]

[a] Department of Life Sciences, Graduate School of Arts and Sciences, The University of Tokyo, 3-8-1 Komaba, Meguro-ku, Tokyo 153-8902, Japan
[b] The Division of Molecular Pathology, Institute of Medical Science, The University of Tokyo, 4-6-1 Shirokanedai, Minato-ku, Tokyo 108-8639, Japan
[c] Department of Pathology, Faculty of Medicine, Kinki University, 377-2 Ohno-Higashi, Osaka-Sayama, Osaka 589-8511, Japan
[d] The Integrated Center for Mass Spectrometry, Kobe University Graduate School of Medicine, 7-5-1 Kusunoki-cho, Chuo-ku, Kobe 650-0017, Japan
[e] Division of Medical Informatics and Bioinformatics, Kobe University Hospital, 7-5-2 Kusunoki-cho, Chuo-ku, Kobe 650-0017, Japan

ARTICLE INFO

Article history:
Received 21 November 2011
Available online 7 December 2011

Keywords:
CADM1
ADAM10
γ-Secretase
Shedding
RIP
Tumor suppressor gene

ABSTRACT

Cell adhesion molecule 1 (CADM1) is a type I transmembrane glycoprotein expressed in various tissues. CADM1 is a cell adhesion molecule with many functions, including roles in tumor suppression, apoptosis, mast cell survival, synapse formation, and spermatogenesis. CADM1 undergoes membrane-proximal cleavage called shedding, but the sheddase and mechanisms of CADM1 proteolysis have not been reported. We determined the cleavage site involved in CADM1 shedding by LC/MS/MS and showed that CADM1 shedding occurred in the membrane fraction and was inhibited by tumor necrosis factor-α protease inhibitor-1 (TAPI-1). An siRNA experiment revealed that ADAM10 mediates endogenous CADM1 shedding. In addition, the membrane-bound fragment generated by shedding was further cleaved by γ-secretase and generated CADM1-intracellular domain (ICD) in a mechanism called regulated intramembrane proteolysis (RIP). These results clarify the detailed mechanism of membrane-proximal cleavage of CADM1, suggesting the possibility of RIP-mediated CADM1 signaling.

1. Introduction

Cell adhesion molecule 1 (CADM1) is a 100–120-kDa multifunctional cell adhesion molecule. CADM1 is a member of the immunoglobulin superfamily and is a type I transmembrane glycoprotein. The extracellular domain of CADM1 undergoes homophilic or heterophilic interaction with necl-1, nectin-3, and CRTAM (class-I MHC-restricted T cell-associated molecule) [1], whereas the intracellular domain interacts with DAL-1 via its band 4.1 binding domain [2] and with pals2 [3] and MPP3 [4] via its PDZ binding domain. CADM1 is expressed in various tissues and organs, including the brain, mast cells, testis, and lung [5].

Recently, Tanabe et al. reported that CADM1 undergoes juxtamembrane cleavage in neurons [6]. We reported previously that shedding fragments were found from mast cells [7] and human mesothelioma samples [8]. These observations suggest that CADM1 shedding is a common event. CADM1 shedding seems to regulate adhesion between mesothelial and mesothelioma cells by down-regulating full-length CADM1, thereby regulating the growth and scattering of mesothelioma cells [8]. Tanabe et al. reported that certain isoforms of CADM1 produce a 20-kDa C-terminal fragment and that production of this fragment is inhibited by the broad-spectrum metalloprotease inhibitor TAPI-1. They concluded that CADM1 is shed by an ADAM17-like protease [6]. The ADAM family metalloproteases are the major membrane-bound sheddases, which are responsible for shedding of many membrane protein substrates. Among the family members, ADAM10 and ADAM17 are the major sheddases and have large numbers of known substrates. After shedding, some membrane proteins undergo a secondary cleavage within the membrane mediated by γ-secretase. For example, Notch, ErbB4, and amyloid precursor protein (APP) are cleaved by γ-secretase [9]. The γ-cleavage product, the intracellular domain (ICD) of the substrate, often acts as a transcriptional regulator. ICDs of Notch and other γ-secretase substrates, such as CD44 [10] and APP [11], act as nuclear signaling molecules that regulate gene expression.

In this study, we focused on CADM1 proteolysis. The aim of this study was to characterize the sheddase of CADM1 and to examine proteolysis events occurring on the CADM1 molecule. Our results

* Corresponding author at: Department of Pathology, Faculty of Medicine, Kinki University, 377-2 Ohno-Higashi, Osaka-Sayama, Osaka 589-8511, Japan. Fax: +81 72 360 2028.
E-mail address: aito@med.kindai.ac.jp (A. Ito).
[1] Present address: Department of Molecular Cell Science, Graduate School of Agricultural Science, Tohoku University, 1-1 Tsutsumidori Amamiya-machi, Aoba-ku, Sendai, Miyagi 981-8555, Japan.

0006-291X/$ - see front matter © 2011 Elsevier Inc. All rights reserved.
doi:10.1016/j.bbrc.2011.11.140

indicated that CADM1 shedding is catalyzed by a protease associated with the cell membrane, and ADAM10 endogenously sheds CADM1. Furthermore, we discovered γ-cleavage of CADM1, which is catalyzed by γ-secretase. These results provide a possible signal-transduction mechanism involving regulated intramembrane proteolysis (RIP).

2. Materials and methods

2.1. Reagents and antibodies

TAPI-1, *N*-[*N*-(3,5-difluorophenacetyl-L-alanyl)]-(*S*)-phenylglycine t-butyl ester (DAPT), and L-685,458 were purchased from Calbiochem (San Diego, CA). Phorbol-12-myristate-13-acetate (PMA) was purchased from Wako (Osaka, Japan). Phenylmethylsulfonyl fluoride (PMSF) and protease inhibitor cocktail (cat.# P8340) were purchased from Sigma (St. Louis, MO).

Anti-CADM1-cyto antibody was generated according to the method described by Wakayama et al. [12]. This antibody recognizes the C-terminal 20 amino acids of CADM1. Anti-CADM1-ecto antibody (3E1) is our original as described previously [13]. This antibody recognizes 2nd Ig domain in the ectodomain. Peroxidase-conjugated secondary antibodies were purchased from Cell Signaling Technology (Danvers, MA).

2.2. In vitro assay of CADM1 shedding

Confluent HEK293 cells were harvested and homogenized in buffer P (20 mM PIPES-KOH pH 7.0, 140 mM KCl, 250 mM sucrose) at 4 °C. The homogenized cells were centrifuged at 800*g* for 10 min to remove the nuclei and cell debris. The supernatant was then ultracentrifuged at 100,000*g* for 1 h, and the resulting pellet was washed with buffer P and ultracentrifuged again at 100,000*g* for 1 h. The resulting pellet (the membrane fraction) was resuspended in buffer P and stored at −80 °C until use.

This membrane fraction was incubated at 37 °C for 1.5 h with the indicated concentrations of protease inhibitors or vehicle only (DMSO, 0.2% for TAPI-1, 1% for PMSF and protease inhibitor cocktail), and the reaction was stopped by addition of 2× sample buffer and boiling for 5 min. These samples were subjected to Western blotting analysis using anti-CADM1-cyto antibody.

2.3. Western blotting analysis

SDS–PAGE and Western blotting were performed according to the standard reducing SDS–PAGE and Western blotting protocols. For detection of CADM1-ICD, samples were separated by Tris–tricine SDS–PAGE and transferred onto Immobilon-P membranes (Millipore, Billerica, MA). The membranes were boiled in PBS for 5 min after transfer and then subjected to blocking, antibody treatments, and subsequent procedures.

2.4. Transfection of siRNA and expression vectors

siRNA (Stealth Select RNAi) specific for human ADAM10 (HSS100167), ADAM17 (HSS110435), and control siRNA (Stealth RNAi negative control low GC duplex, 12935-200) were purchased from Invitrogen (Carlsbad, CA). Saos-2 cells at 40–50% confluence were transfected with siRNAs using Lipofectamine RNAiMax Transfection Reagent (Invitrogen) according to the manufacturer's instructions. After 96 h of incubation, cells were harvested, and the cell lysates were analyzed by Western blotting.

2.5. Cell culture

cDNA encoding mouse-CADM1 (GenBank ID: AB052293) was cloned into the expression vector pCX4-bsr and confirmed by DNA sequencing (pCX4bsr-CADM1) [7]. COS7 cells and NIH3T3 cells were transfected with the pCX4bsr-CADM1 vector, and blasticidin-resistant cells were selected by continuing the culture in the presence of blasticidin (3 μg/mL) for 4 weeks (COS7-mCADM1 and NIH3T3-mCADM1). MEF and nicastrin$^{-/-}$ MEF cells were kind gifts from Dr. Philip C. Wong (The Johns Hopkins University), and presenilin 1/2 double knockout MEF was a kind gift from Dr. Bart De Strooper (Vlaams Instituut voor Biotechnologie). These cells, HEK293, and human osteosarcoma Saos-2 were maintained in DMEM supplemented with 10% fetal bovine serum and penicillin/streptomycin. In γ-secretase inhibitor assay, confluent COS7-mCADM1 cells were treated with 200 ng/mL PMA for 2 h, and then γ-secretase inhibitor (1 μM DAPT or 1 μM L-685,458) or vehicle (DMSO) was added. After incubation for the indicated times, cells were harvested, and the cell lysates were analyzed by Western blotting.

2.6. Mass spectrometric analysis

NIH3T3-mCADM1 cells were harvested, and the membrane fraction extract was prepared using Subcellular Proteome Extraction Kit (Merck, Whitehouse Station, NJ). The membrane fraction extract was concentrated using Amicon Ultra 15 (Millipore) and then immunoprecipitated using anti-CADM1cyto antibody. The precipitate was mixed with sample buffer and subjected to SDS–PAGE. The gel was stained with EZ-Blue (Sigma), and the alphaCTF band was cut out. In-gel digestion with chymotrypsin was performed according to the published methods [14,15]. The digested peptides were subjected to liquid chromatography (LC)/MS/MS analysis on a Q-Tof2 quadrupole/time-of-flight (TOF) hybrid mass spectrometer (Micromass, Manchester, UK) interfaced with a capillary reversed-phase liquid chromatography system (Micromass CapLC system) as described previously [14]. The MS/MS data were analyzed with Mascot MS/MS Ion Search (version 2.1.6; Matrix Science Ltd., London, UK) to assign the obtained peptides to the NCBI non-redundant database (NCBInr 20060718; 3784285 sequences) as described previously [14].

3. Results

3.1. CADM1 shedding is promoted by phorbol ester

To study shedding of CADM1, we first generated a stable COS7 cell line expressing murine CADM1 (COS7-mCADM1). Several CADM1-derived bands, including bands of approximately 15 and 35 kDa, were detected from COS7-mCADM1 lysate by Western blotting with an antibody that recognizes the C-terminal of CADM1. We refer to the 15- and 35-kDa fragments as alphaCTF (C-terminal fragment) and betaCTF, respectively. AlphaCTF is likely to be the same shedding fragment of CADM1 reported previously [6], and betaCTF is another fragment of CADM1. As shedding of some other membrane proteins is promoted by phorbol esters such as PMA, we examined the effects of PMA treatment on CADM1 shedding (Fig. 1A) and found that alphaCTF was increased after PMA treatment. On the other hand, no apparent changes were observed in the 35-kDa band, which was thought to be another cleaved fragment of CADM1.

We next concentrated CADM1 alphaCTF by immunoprecipitation and determined the cleavage site by LC/MS/MS. Following SDS–PAGE, the gel slice containing the alphaCTF band was excised

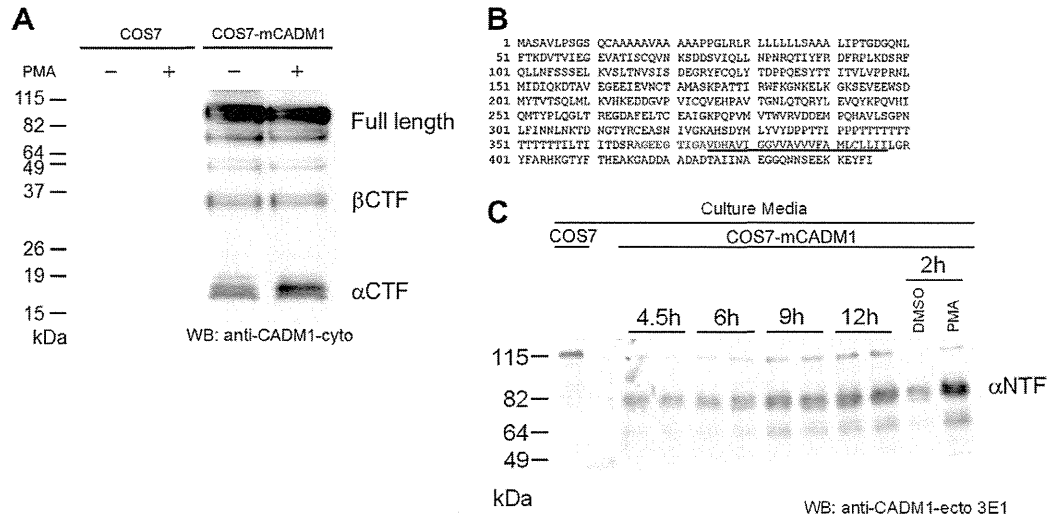

Fig. 1. Ectodomain shedding of CADM1, (A) COS7-mCADM1 cells were treated with 200 ng/mL PMA or vehicle alone for 30 min and then harvested. Cell lysates were analyzed by Western blotting using anti-CADM1-cyto antibody. (B) Determination of the cleavage site of CADM1 shedding. The peptide detected by LC/MS/MS is indicated in red, and the transmembrane region is underlined. (C) Culture medium of subconfluent COS7-mCADM1 cells was changed to serum-free medium and incubated for the indicated times (duplicate results are shown). To evaluate PMA-dependent secretion, 200 ng/mL PMA or vehicle (DMSO) was added to the serum-free medium and incubated for 2 h. The medium was then harvested and concentrated by TCA precipitation. The precipitate was analyzed by Western blotting using anti-CADM1-ecto antibody 3E1. (For interpretation of the references to color in this figure legend, the reader is referred to the web version of this article.)

and cleaved with chymotrypsin in the gel. LC/MS/MS detected a peptide fragment with an N-terminus generated by proteases other than chymotrypsin (Fig. 1B). This observation suggested that the N-terminus of the detected peptide was generated by shedding. The cleavage site was between R365 and A366, nine amino acid residues from the predicted transmembrane region in the extracellular domain. This result predicted that alphaCTF is an 80 amino acids fragment. Larger apparent molecular weight of this fragment on Western blotting is probably due to O-linked glycosylation. This result also predicted that N-terminal fragments are released into the culture medium after shedding and that PMA treatment would increase this release. Therefore, we analyzed the culture media by Western blotting and found that there was indeed a CADM1 fragment corresponding in size to NTF after cleavage that produces alphaCTF. As expected, we also found that PMA treatment increased the amount of CADM1 fragments in the culture medium (Fig. 1C).

Taken together, these results suggest that CADM1 shedding produces alphaCTF and a corresponding extracellular fragment, that cleavage occurs in the membrane-proximal region of CADM1 extracellular domain, and that shedding is promoted by PMA.

3.2. CADM1 shedding was detected in an in vitro membrane-fraction incubation assay

CADM1 shedding was previously shown to be inhibited by TAPI-1, a broad-spectrum inhibitor that targets many metalloproteases such as ADAMs and MMPs. Among them, those with transmembrane domains are known to shed a large number of transmembrane substrates.

To obtain further information about CADM1 sheddase, we performed an *in vitro* assay using total cell membrane fraction and focusing on membrane-bound proteases.

To avoid artifacts due to overexpression of CADM1, we prepared total membrane fraction from HEK293 cells, which constitutively express endogenous CADM1. The total membrane fraction prepared by ultracentrifugation was incubated. The level of alphaCTF increased after incubation, whereas that of full-length CADM1 decreased (Fig. 2A). BetaCTF was barely detectable in this preparation. The increase in the 15-kDa band was inhibited by addition of TAPI-1 (Fig. 2A and B), as reported previously by Tanabe et al. [6], who added TAPI-1 to neuronal cells. Serine, cysteine, and aspartic protease inhibitors showed no inhibitory effect on CADM1 shedding (Fig. 2C). Thus, we could reconstitute shedding of CADM1 *in vitro* by incubation of the membrane fraction and could characterize the sensitivity to protease inhibitors using this method. These results indicated that a membrane-associated metalloprotease possesses CADM1 shedding activity.

3.3. CADM1 shedding is mediated by the metalloprotease ADAM10

Many membrane molecules undergo shedding, and ADAM10 and ADAM17 were reported to be two major membrane-associated sheddases. An siRNA approach was employed here to investigate whether ADAM10 and/or ADAM17 cleaved CADM1. The Saos-2 human osteosarcoma cell line, which shows high-level expression of endogenous ADAM10, was used in this assay. The siRNAs used downregulated the mature form of targeted ADAMs as well as the proform (Fig. 3A). Knockdown of ADAM10 expression decreased the amount of alphaCTF, whereas the knockdown of ADAM17 had no effect on the amount of alphaCTF. Furthermore, ADAM10 knockdown abolished PMA-dependent accumulation of alphaCTF (Fig. 3B). These observations indicated that CADM1 is cleaved endogenously by the metalloprotease ADAM10, and PMA-dependent cleavage of CADM1 is also mainly mediated by ADAM10.

3.4. γ-Secretase-like cleavage is abrogated in the presence of γ-secretase inhibitors and in γ-secretase KO cells

Following membrane-proximal cleavage, similar to CADM1 shedding, some membrane proteins undergo a second cleavage mediated by γ-secretase. To determine whether CADM1 is cleaved by γ-secretase, we examined the effects of γ-secretase inhibition on the amounts of cleaved CADM1 fragments after induction of shedding by PMA. COS7-mCADM1 cells were treated with PMA or vehicle alone and then treated with γ-secretase inhibitor (DAPT or L-685,458) or vehicle alone. The amount of alphaCTF increased in

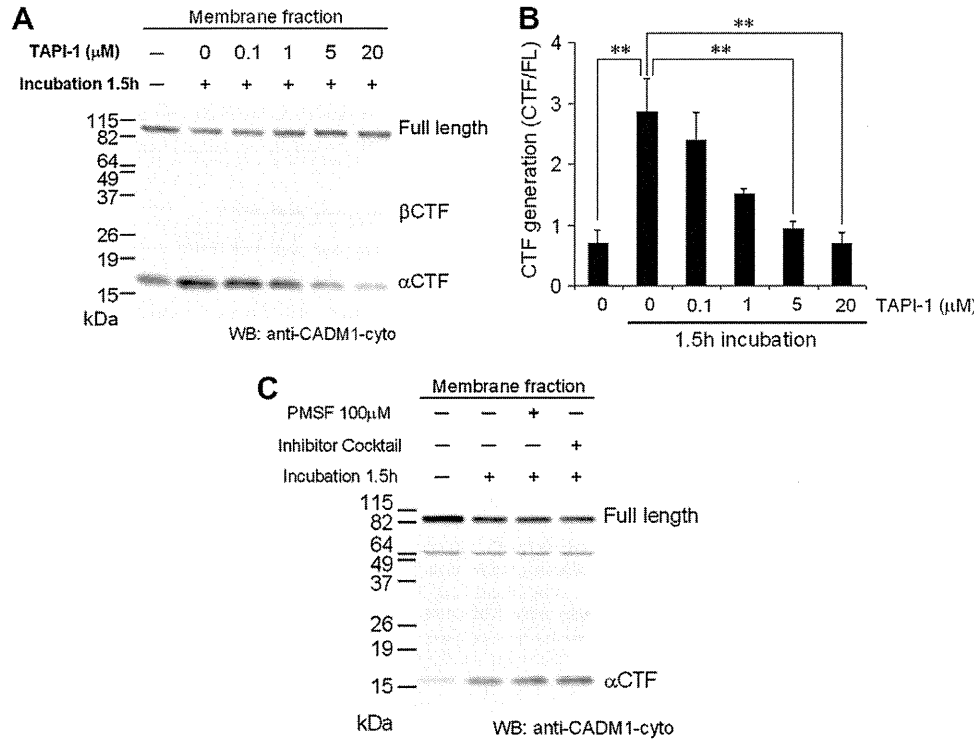

Fig. 2. *In vitro* CADM1 shedding assay. (A–C) Membrane fraction was obtained from HEK293 cells as described in Section 2. The membrane fraction was incubated with the indicated concentration of protease inhibitors and subjected to Western blotting analysis using anti-CADM1-cyto antibody. The results of densitometric analysis of CADM1-CTF generation in (A) are shown in (B). CTF generation was calculated as CTF/full-length ratio by densitometric analysis. Results were obtained from three independent experiments and are expressed as means ± SEM. Data were analyzed by one-way analysis of variance followed by Dunnett's multiple comparison test. **Statistically significant compared with "1.5 h, 0 μM TAPI-1" ($p < 0.01$). The inhibitor cocktail in (C) was from Sigma (P8340).

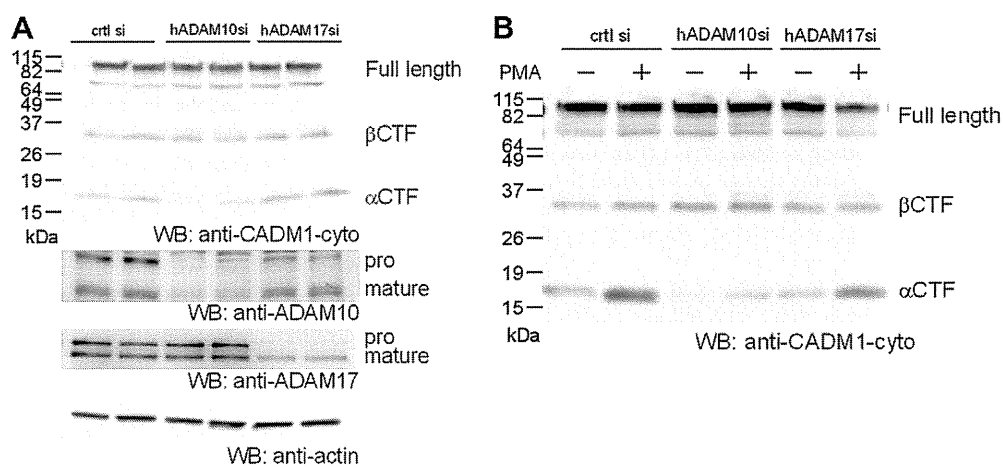

Fig. 3. Knockdown of ADAM10 decreases CADM1-CTF level. (A) Saos-2 cells were transfected with siRNAs against ADAM10 or ADAM17 or with control siRNA. Cells were harvested after 96 h of incubation. Cell lysates were subjected to Western blotting analysis using anti-CADM1-cyto antibody (duplicate results are shown). In (B), cells were treated with 200 ng/mL PMA or vehicle only (DMSO) for 4 h and then harvested.

the presence of γ-secretase inhibitor (Fig. 4A), indicating γ-secretase-dependent degradation of alphaCTF. This finding suggested that alphaCTF was cleaved by γ-secretase into a cytosolic fragment, CICD (CADM1 intracellular domain). With membrane boiling and prolonged exposure, a CADM1-derived band of nearly 6 kDa was detected (Fig. 4A). Membrane boiling contributes to the detection of this 6 kDa fragment, and it is necessary to boil the membrane for the detection of obvious CICD band. The amount of this fragment was decreased with γ-secretase inhibitor treatment, consistent with alphaCTF accumulation (Fig. 4A). γ-Secretase cleaves its substrates within the cell membrane at around three amino acids from the cytosolic end of the transmembrane region of the substrate and generates a fragment with an intact cytoplasmic domain. The theoretical molecular weight of CADM1 cytoplasmic domain is 5.3 kDa. This fragment is the cleavage product of CADM1 generated by γ-secretase. These results suggest that alphaCTF is cleaved by γ-secretase and generates CICD fragments.

We employed another approach to further confirm this possibility. γ-Secretase consists of four proteins, presenilin, nicastrin, Aph-1, and Pen-2, all of which are indispensable for its activity. We used

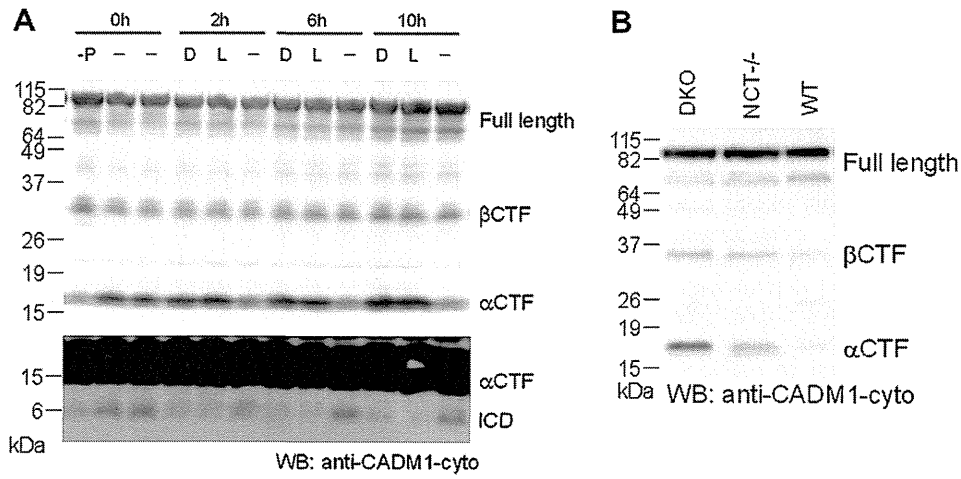

Fig. 4. CADM1-ICD generation is dependent on γ-secretase. (A) COS7-mCADM1 cells were pretreated with 200 ng/mL PMA or vehicle alone (–P: DMSO) for 2 h, and subsequently treated with γ-secretase inhibitors (D: 1 μM DAPT or L: 1 μM L-685,458) or vehicle alone (–: DMSO) and incubated for the indicated times. (B) Cultured cells of two mouse embryonic fibroblast (MEF) cell lines lacking γ-secretase activity and a wild-type MEF cell line were harvested. Cell lysates were analyzed by Western blotting using anti-CADM1-cyto antibody.

two MEF cell lines with no γ-secretase activity, one lacking presenilin-1 and presenilin-2 (PSDKO) and another lacking nicastrin ($NCT^{-/-}$) [16,17]. On Western blotting analysis, the alphaCTF level was increased in γ-secretase KO MEFs but not in wild-type MEFs (Fig. 4B). These results were consistent with those of γ-secretase inhibitor assay, indicating that alphaCTF is processed into CICD by γ-secretase.

4. Discussion

Many previous studies have addressed the various functions of CADM1. Genetic analyses of human cancer suggest that CADM1 has potent tumor-suppressor activity. CADM1 was also shown to suppress tumorigenicity in mouse models, to induce apoptosis, and to suppress cell proliferation *in vitro* [18]. However, the molecular mechanisms underlying these and other functions are largely unknown. In the present study, we focused on membrane protein proteolysis, which may modulate or mediate the functions of such proteins. A previous study indicated that certain CADM1 isoforms are shed due to the action of a ADAM17-like protease [6]. We examined CADM1 proteolysis in more detail, and here we demonstrated the two-step mechanism of CADM1 proteolysis including shedding and RIP with identification of the cleavage site of shedding, sheddase, and subsequent γ-cleavage.

We first demonstrated enhancement of CADM1 shedding by PMA and accumulation of the cleaved extracellular fragment in the medium. A soluble CADM1 isoform was shown to elicit directional neurite extension up a CADM1 concentration gradient [19]. According to the cleavage site determined here, the whole sequence of the soluble isoform was contained within the shed fragment with the exception of two amino acids near the isoform-specific C-terminus. These observations suggest that CADM1 extracellular fragment may also serve as a neurite attractant with a regulated mechanism of secretion. Unexpectedly, although betaCTF was abundant in several cell lines, betaNTF was much less abundant than alphaNTF in the culture medium of the same cells. An as-yet-unknown cellular system may retain and degrade the "extracellular" fragment within the cells.

We developed an *in vitro* shedding assay and demonstrated that CADM1 shedding could occur not only in the intact cell but also in the isolated membrane fraction. This method can be used as a novel *in vitro* assay for ectodomain shedding. To date, *in vitro* shedding assays have mostly been performed by the addition of purified protease to the membrane fraction, which contains the substrate. Our method is closer to physiological conditions because the endogenous localization of a protease and its substrate should be intact. Using this method, we showed here that shedding of CADM1 was directly mediated by a membrane-bound metalloprotease. TAPI-1 was also shown to have an inhibitory effect on CADM1 shedding, consistent with previous findings [6]. Furthermore, the results of siRNA experiments indicated that ADAM10, but not ADAM17, is a potent endogenous sheddase of CADM1. In contrast, previous studies showed that nectin-1 and nectin-4, both of which are adhesion molecules related to CADM1, are cleaved by ADAM10 and ADAM17, respectively [20,21]. ADAM10 is a well-known sheddase that cleaves many other adhesion molecules. Although no consensus cleavage sequence is known for ADAM10, this molecule cleaves its substrate at a site 8–20 amino acids from the transmembrane region in its ectodomain [22]. In the present study, the cleavage site for CADM1 shedding was determined to be nine amino acids from the transmembrane region by MS analysis, indicating that shedding of CADM1 is similar to that of other known cell-surface molecules mediated by ADAM10.

We next showed that CADM1 undergoes γ-secretase-mediated cleavage and generates CADM1-ICD using inhibitors or γ-secretase-deficient cell lines. A previous study indicated that nectin-1α is also cleaved by γ-secretase-like activity to generate ICD [23]. This process is known to involve proteolytic cleavage called RIP, in which removal of the ectodomain by shedding is necessary for the second cleavage catalyzed by γ-secretase [9]. Our data suggested that the substrate of γ-cleavage is the membrane-bound shedding product alphaCTF, consistent with the known mechanism of RIP. Compared with alphaCTF, the amount of CICD fragment is very small, and the difference between the amount of the fragment with and without inhibitor treatment was small. This is probably because of the rapid degradation of CICD, as many other ICD fragments generated by γ-secretase, including Notch ICD, are known to be rapidly degraded in a proteasome-dependent manner [23].

ICD often acts as a signal transducer. Nuclear staining for CADM1 was observed on microscopic analysis using C-terminal GFP-tagged CADM1 or antibody against CADM1 cytosolic domain ([1] and unpublished data). CASK, a protein that binds to CADM1 cytoplasmic domain, is partially localized to the nucleus and interacts with the T-box transcription factor Tbr-1, inducing transcription of genes including NR2b [24]. CADM1-ICD may be transported into the nucleus together with CASK and may modulate